Enhanced superconductivity in proximity to peaks in densities of states

Joshua Althüser, * Ilya M. Eremin, † and Götz S. Uhrig ‡

Condensed Matter Theory, TU Dortmund University, Otto-Hahn Straße 4, 44227 Dortmund, Germany and Theoretische Physik III, Ruhr-Universität Bochum, 44801 Bochum, Germany

(Received 12 December 2025; accepted 21 August 2026; published 8 September 2026)

For the BCS theory of superconductivity, the electron-phonon interaction is transformed to an attractive electron-electron interaction in the vicinity of the Fermi energy only. At the same time, its formal derivation using a unitary transformation reveals that the electrons attract one another whenever their energies do not differ by more than the phonon energy ω_{D}, independent of closeness to the Fermi energy. Consequently, the order parameter becomes finite even away from the Fermi level. Yet, for small interactions, its magnitude is usually small and can be safely ignored, justifying the BCS approximation. Intriguingly, we find that an accumulation of density of states at an energy $\varepsilon_{\mathrm{peak}}$ in proximity to the Fermi energy induces a significant order parameter magnitude around $\varepsilon_{\mathrm{peak}}$, which exceeds the one at E_{F} for moderate coupling strengths. This strong enhancement is heralded by the softening of an additional collective mode, which resembles a second phase transition. We predict measurable signatures in the thermodynamic and spectroscopic responses to this unexpected phenomenon, guiding future experimental searches for it. Finally, we demonstrate that these signatures remain robust upon including a phenomenological Coulomb repulsion, indicating that the enhancement is not an artifact of the idealized model.

DOI: 10.1103/xbsf-8l6q

I. INTRODUCTION

The weak-coupling regime of superconductors is well understood in the framework of the BCS theory [1]. The essential result is that the superconducting (SC) instability is determined by the product of the attractive coupling times the electronic density of states (DOS) at the Fermi energy, and the transition temperature becomes higher by increasing at least one of them. The relevant physics is given by what happens in an energetically narrow layer around the Fermi energy, and its width is given by the characteristic phononic Debye frequency ω_{D}. Since then, strong-coupling superconductors have been a central focus of research for decades and continue to incite great interest [2–11], striving to realize high-T_c superconductivity and the limits beyond the pure weak-coupling scenario.

In conventional superconductors, the attractive electron-electron interaction is derived from the electron-phonon coupling by a unitary transformation [12–16] if one does not resort to an explicit description of the phonon degrees of freedom as well [2]. The standard weak-coupling form of the attraction between an electron at energy ε and one at energy ε' reads

$$g_{\mathrm{BCS}}(\varepsilon,\varepsilon') = -\frac{g_{\mathrm{BCS}}}{2\rho_{\mathrm{F}}}\Theta(\omega_{\mathrm{D}}-|\varepsilon-E_{\mathrm{F}}|)\Theta(\omega_{\mathrm{D}}-|\varepsilon'-E_{\mathrm{F}}|), \tag{1}$$

where g_{BCS} is second order in the electron-phonon coupling M and ρ_{F} is the DOS at the Fermi energy. Throughout this article, we will use natural units $\hbar = k_{\mathrm{B}} = 1$, and g_{BCS} is defined to be dimensionless.

However, even in second order in M, this expression appears to be a stark approximation. Avoiding it yields expressions that depend on the difference $\varepsilon-\varepsilon'$ only. The simplest form is rigorously derived via a continuous unitary transformation based on an infinitesimal generator depending on the sign of $\varepsilon-\varepsilon'\pm\omega_{\mathrm{D}}$, yielding

$$g(\varepsilon,\varepsilon') = -\frac{g}{2\tilde{\rho}}\Theta(\omega_{\mathrm{D}}-|\varepsilon-\varepsilon'|) \tag{2}$$

in second order of the electron-phonon interaction without any further approximation [17]. A sketch of the derivation is provided in Appendix A. Here, we defined the dimensionless coupling strength g and the average DOS around the Fermi edge $\tilde{\rho} := 1/(2\omega_{\mathrm{D}})\int_{E_{\mathrm{F}}-\omega_{\mathrm{D}}}^{E_{\mathrm{F}}+\omega_{\mathrm{D}}} d\varepsilon\,\rho(\varepsilon)$ so that the formula can be employed also in case of divergences or other strongly fluctuating DOS. We stress that the dimensionless coupling g can easily take values up to $\mathcal{O}(1)$, although it results from a perturbative expansion in the electron-phonon coupling M. The reason is that the expansion in M requires M/ω_{D} to be small, but does not prevent $M^2\tilde{\rho}/\omega_{\mathrm{D}}$ from being of order unity or larger [8].

Note that the extension of the BCS theory toward inclusion of retardation effects and Coulomb repulsion (Eliashberg

*Contact author: joshua.althueser@tu-dortmund.de
†Contact author: ilya.eremin@ruhr-uni-bochum.de
‡Contact author: goetz.uhrig@tu-dortmund.de

theory) still relies on the BCS assumption that the attractive part of the interaction involves quasiparticles in the vicinity of the Fermi level, yet the interaction is repulsive outside of this region [18]. In contrast, the energy-difference-dependent interaction, which we will employ, allows for attractive Cooper-pairing interaction due to phonons beyond the immediate vicinity of the Fermi level. We recall that even the originally derived form of the Fröhlich interaction does not impose a cutoff energy at a certain distance from the Fermi level. For the choice (2), we show that the order parameter in the superconducting phase is finite even far away from the Fermi energy, yet with decreasing modulus upon increasing energetic distance $|\epsilon - E_F|$ [11,13,14].

An intriguing scenario with unexpected qualitative features arises if a significant accumulation, i.e., a peak, of DOS is present at $\varepsilon_{\text{peak}}$ in energetic proximity to the Fermi energy. The distance in energy from E_F does not need to be smaller than the Debye energy ω_D, but $\varepsilon_{\text{peak}}$ can be several ω_D away for moderate values of g. Then, we find a sudden increase in the superconducting order parameter $\Delta(\varepsilon \approx \varepsilon_{\text{peak}})$. Correspondingly, it is also accompanied by a strongly enhanced mean-field critical temperature. The whole phenomenon appears as a function of temperature in two stages strongly resembling two consecutive phase transitions. It is heralded by the softening of an additional collective mode, which should be detectable spectroscopically.

The article is organized as follows. In Sec. II, the model is introduced. The numerical results are presented in Sec. III, where we first ignore the effect of the Coulomb repulsion and then discuss how its inclusion affects our initial findings. We conclude and provide an outlook in Sec. VI.

II. MODEL

We consider the following Hamiltonian describing the electronic subsystem with electron-phonon interaction:

$$\mathcal{H} = \sum_{\boldsymbol{k}\sigma}(\varepsilon_{\boldsymbol{k}} - \mu)\hat{c}^\dagger_{\boldsymbol{k},\sigma}\hat{c}_{\boldsymbol{k},\sigma} + \frac{1}{N}\sum_{\boldsymbol{k}\boldsymbol{k}'\sigma} g(\boldsymbol{k},\boldsymbol{k}')\hat{c}^\dagger_{\boldsymbol{k},\sigma}\hat{c}^\dagger_{-\boldsymbol{k},-\sigma}\hat{c}_{-\boldsymbol{k}',-\sigma}\hat{c}_{\boldsymbol{k}',\sigma}, \tag{3}$$

where $\hat{c}^{(\dagger)}_{\boldsymbol{k},\sigma}$ annihilate (create) an electron with momentum $\boldsymbol{k}$ and spin σ, $\varepsilon_{\boldsymbol{k}}$ is the single-particle dispersion, μ is the chemical potential, and N the number of lattice sites. We choose the hopping constant such that $\varepsilon \in [-W, W]$. For simplicity, we assume a single optical phonon branch at the Debye frequency $\omega_{\boldsymbol{q}} \equiv \omega_D$ and a constant electron-phonon coupling [11]. The chemical potential $\mu(T)$ is computed self-consistently such that the filling is kept constant; see further details in Appendix B. We initialize the system with the Fermi energy E_F of the would-be normal state at $T = 0$. Note that $g(\boldsymbol{k},\boldsymbol{k}') \leqslant 0$. We employ $\omega_D = 0.04W$ and $E_F = -0.5W$ here; Secs. C and D provide results for different parameters as well.

We consider a generic Bravais lattice, here the body-centered cubic (bcc) lattice, with nearest-neighbor hopping. This DOS is plotted in Fig. 1(a) [19]. A large fraction of its weight is located around the logarithmic divergence at $\varepsilon = 0 = \varepsilon_{\text{peak}}$. We stress that a divergence is not required for the advocated phenomenon. The only requirement is that a large weight is located away from the Fermi level. In Appendix E, we examine such a DOS without a divergence and observe qualitatively the same features.

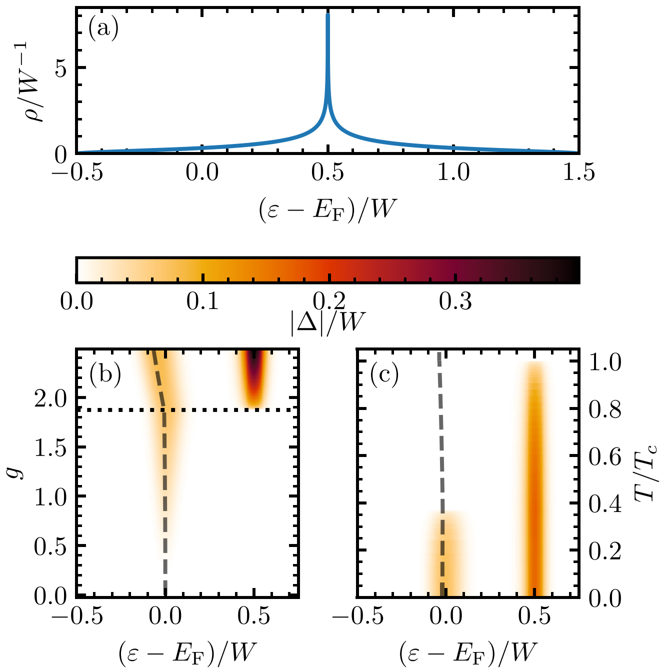

FIG. 1. (a) Calculated DOS ρ of a bcc lattice with nearest-neighbor hopping. (b) Order parameter $\Delta(\varepsilon)$ at $T = 0$ vs the interaction strength g and the bare dispersion ε. The dotted line indicates the interaction strength $g_{\text{enh}} \approx 1.866$ at which the SC order appears at the energy position of the logarithmic divergence. The dashed line marks the chemical potential $\mu(T)$. (c) Order parameter $\Delta(\varepsilon)$ vs temperature T at $g = 2 > g_{\text{enh}}$. For rising T, the order parameter first vanishes at $E_F = -0.5W$, but remains finite at $\varepsilon = 0$. At T_c, superconductivity vanishes.

In order to assess how additional interactions, such as Coulomb interactions, influence the scenario of enhanced superconductivity, we add a local Hubbard-like interaction projected onto the pairing channel

$$\mathcal{H}_C = \frac{U}{2\tilde{\rho}}\frac{1}{N}\sum_{\boldsymbol{k}\boldsymbol{k}'\sigma}\hat{c}^\dagger_{\boldsymbol{k},\sigma}\hat{c}^\dagger_{-\boldsymbol{k},-\sigma}\hat{c}_{-\boldsymbol{k}',-\sigma}\hat{c}_{\boldsymbol{k}',\sigma}. \tag{4}$$

Structurally, this interaction has the same form as the one proposed by Morel and Anderson. In their derivation, Morel and Anderson considered a parabolic electron dispersion relation. This assumption is well justified for good metals, where typical values are $U \approx 0.1$ [20].

We compute the thermodynamic properties of the system, such as the heat capacity C_V and the critical transition temperature T_c, by a standard self-consistent mean-field decoupling of the interaction term. The expectation values $\langle \hat{c}^\dagger_{\boldsymbol{k},\uparrow}\hat{c}^\dagger_{-\boldsymbol{k},\downarrow}\rangle$, and hence, the order parameter

$$\Delta(\varepsilon) = -2\int d\varepsilon' \left(\frac{U}{2\tilde{\rho}} + g(\varepsilon,\varepsilon')\right)\rho(\varepsilon')\frac{\Delta(\varepsilon)}{2E(\varepsilon)} \tag{5}$$

depends on the wave vectors only via the bare energy ε so that the DOS suffices to take the lattice into account. Here, $E(\varepsilon) := \sqrt{(\varepsilon - \mu)^2 + \Delta^2(\varepsilon)}$ is the quasiparticle dispersion. To determine T_c, we solve the mean-field equations fully self-consistently starting at low temperatures and increasing T until the order parameter vanishes. Then, we fit the maximum of the order parameter to $\sqrt{T-T_c}$ for temperatures slightly below T_c to obtain the proper value of T_c. To this end, the DOS is discretized by an energy mesh with 10 000 equidistant points.

III. RESULTS

We first present the results without taking the Coulomb repulsion Eq. (4) into account; its effects are discussed later. Figure 1(b) depicts the order parameter $\Delta(\varepsilon)$ at $T=0$. The interaction strength g is shown along the y axis, while the color scale represents $|\Delta|$. The dashed line indicates the chemical potential μ to guide the eye. Although $\mu(T)-E_{\mathrm{F}}$ is generally finite, it remains comparatively small; a detailed discussion of the chemical potential as a function of g and T is given in Appendix B. A complementary momentum-space representation of the order parameter is presented in Appendix F.

For weak and intermediate coupling strengths, the superconducting order parameter is confined to the vicinity of the Fermi energy, as expected from conventional BCS theory. Above a crossover interaction strength g_{enh}, however, a second region of finite order develops around the pronounced peak in the density of states at ε_p. In the following, we refer to the superconducting order localized around the chemical potential as the *conventional order*, whereas the additional order near ε_p is denoted as the *enhanced order*. The latter originates from the substantial spectral weight accumulated at the DOS peak. The corresponding contribution to the self-consistency equation,

$$\Delta(\varepsilon_p)=\frac{g}{\tilde{\rho}}\int_{\varepsilon_p-\omega_{\mathrm{D}}}^{\varepsilon_p+\omega_{\mathrm{D}}}\mathrm{d}\varepsilon'\rho(\varepsilon')\frac{\Delta(\varepsilon')}{2E(\varepsilon')},\tag{6}$$

becomes large despite the large quasiparticle energies $E(\varepsilon')$. This mechanism is a direct consequence of considering an interaction with finite energy transfer. For the present model parameters, we obtain the value $g_{\mathrm{enh}}\approx 1.866$.

For the parameters considered here, the conventional and enhanced order parameters remain energetically separated. Between μ and ε_p, $\Delta(\varepsilon)$ decays exponentially over an interval exceeding ω_{D} and therefore vanishes numerically. Consequently, the crossover regime is exponentially small and appears numerically as a sharp threshold. Nevertheless, we find that their relative phase is not arbitrary, particularly if additional interactions such as the Coulomb repulsion are included (see Sec. IV). Similarly, the crossover regime also becomes discernible.

Once the enhanced order develops, $\Delta(\varepsilon_p)$ rapidly exceeds the order parameter around the Fermi energy. Nevertheless, the minimum quasiparticle excitation energy remains close to the chemical potential because the quasiparticle dispersion $E(\varepsilon)=\sqrt{(\varepsilon-\mu)^2+|\Delta(\varepsilon)|^2}$ is still minimized in the vicinity of the Fermi level. The minimum may be slightly shifted away from $\varepsilon=\mu$ if $\Delta(\varepsilon)$ decreases sufficiently rapidly, as discussed previously [11]. For clarity, we define the true excitation gap $\Delta_{\mathrm{true}}:=\min_\varepsilon E(\varepsilon)$ and distinguish it from the maximum order parameter $\Delta_{\max}:=\max_\varepsilon|\Delta(\varepsilon)|$.

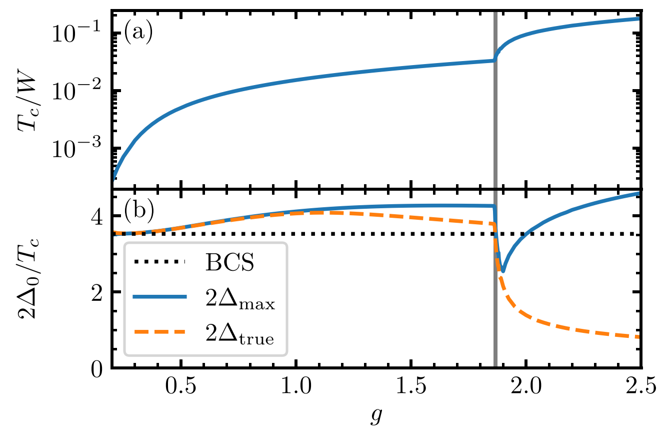

FIG. 2. (a) Calculated critical temperature T_c vs the interaction strength g; note the logarithmic scale on the y axis. From $g=g_{\mathrm{enh}}\approx 1.866$ (gray vertical line) onward, the enhanced order significantly increases T_c. (b) Ratio of the maximum value of the order parameter $\Delta_{\max}:=\max_\varepsilon|\Delta(\varepsilon)|$ (blue solid line) and the energy gap of the quasiparticle dispersion $\Delta_{\mathrm{true}}:=\min_\varepsilon E(\varepsilon)$ (orange dashed line) at $T=0$ relative to T_c vs g. The black dotted line marks the well-known ratio of standard BCS theory (≈3.528) [22].

The evolution with temperature further highlights the distinction between the two superconducting orders. For $g<g_{\mathrm{enh}}$, the order parameter follows essentially conventional BCS behavior apart from moderate quantitative renormalizations. Above the crossover, however, the enhanced order dominates. In particular, the conventional order disappears at a substantially lower temperature than the enhanced one, as illustrated in Fig. 1(c) for $g=2$. This separation of temperature scales immediately suggests pronounced consequences for thermodynamic observables. The most direct consequence is the critical temperature T_c, shown in Fig. 2(a). For weak coupling, where only conventional superconductivity exists, T_c increases gradually with g, reproducing the familiar BCS trend. Upon reaching g_{enh}, however, T_c rises abruptly as the enhanced order becomes established. Although this rapid increase resembles a phase transition, it is not associated with an additional symmetry breaking. Instead, it closely resembles metamagnetic transitions known from magnetic systems [21], motivating the designation *metasuperconducting transition*.

Additional insight is provided by the ratios of the characteristic energy scales to the critical temperature, shown in Fig. 2(b). For weak coupling, both $\Delta_{\max}$ and Δ_{true} reproduce the universal BCS ratio $2\Delta_0/T_c\approx 3.528$ [22]. At intermediate coupling, both ratios increase moderately while Δ_{true} and $\Delta_{\max}$ begin to separate [11]. Once the enhanced order emerges at g_{enh}, both ratios decrease sharply. The ratio $\Delta_{\max}/T_c$ subsequently recovers because $\Delta(\varepsilon_p)$ grows rapidly, whereas $\Delta_{\mathrm{true}}/T_c$ remains small since the minimum quasiparticle gap is not enhanced.

These distinct temperature scales also leave clear signatures in the specific heat, shown in Fig. 3. For $g<g_{\mathrm{enh}}$ (grayscale curves), the system displays essentially renormalized BCS behavior, with the characteristic discontinuity at T_c. In contrast, for $g>g_{\mathrm{enh}}$ (colored curves), the specific heat exhibits two anomalies. The first coincides with the disappearance of the conventional order at the Fermi level, whereas the

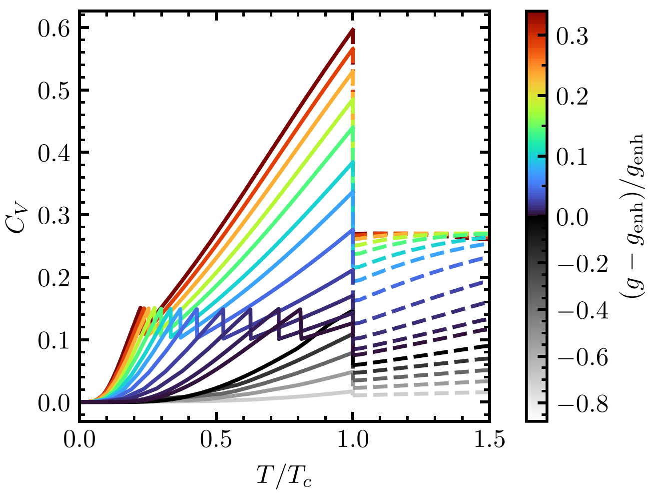

FIG. 3. Calculated specific heat C_V vs temperature T. The colors represent the coupling strengths g according to the color scale. Solid lines refer to the superconducting state, while dashed lines refer to the normal state. For $g < g_{\mathrm{enh}}$ (in grayscale), we observe renormalized BCS behavior. For $g > g_{\mathrm{enh}}$ (colored), unexpected qualitative behavior arises resembling two consecutive phase transitions. The threshold value is $g_{\mathrm{enh}} \approx 1.866$.

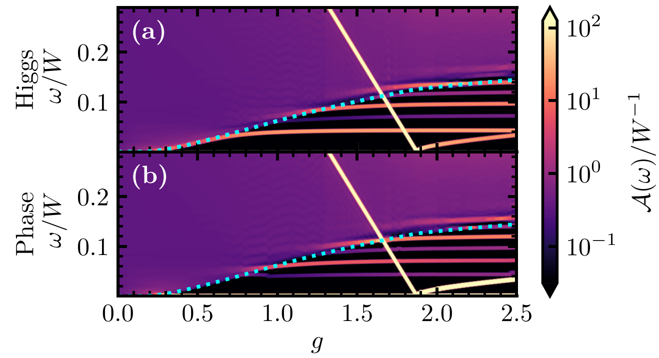

FIG. 4. Calculated spectral functions of (a) $\mathcal{A}_{\mathrm{Higgs}}(\omega)$ and (b) $\mathcal{A}_{\mathrm{Phase}}(\omega)$ represented by the color scale. The energy varies along the y axis, and the interaction strength g along the x axis. The cyan dotted line marks the lower edge of the quasiparticle continuum $2\Delta_{\mathrm{true}}$. The secondary modes found in Ref. [11] are clearly visible. Additionally, a sharp mode rapidly decreases in energy until softening at $g = g_{\mathrm{enh}} \approx 1.866$. δ peaks below the continuum are shown as Gaussian curves of the same weight and width $\sigma = 0.0005W$. The primary phase mode appears at zero energy as a δ' peak since no long-range Coulomb interaction is included; it is plotted as the derivative of a Gaussian curve. The evaluation uses 16 000 equidistant points in ε space.

second marks the superconducting transition at T_c, where the enhanced order finally vanishes. If the conventional and enhanced order parameters overlap energetically—for example, by increasing g or ω_{D}—the lower-temperature discontinuity gradually broadens into a λ-like anomaly (see Sec. IV and Appendixes C and D). A similar rounding is obtained by including the Hubbard-like repulsive interaction U.

Within the present mean-field treatment, the disappearance of the conventional order with persisting enhanced order formally implies a gapless superconducting phase. We do not, however, expect such a phase to persist in realistic materials, because additional interactions—most importantly the Coulomb interaction—couple the superconducting order over different energy scales [11,14,20,23–25]. Our calculations including a Hubbard-like repulsion indeed support this picture, as discussed in Sec. IV. While the true long-range Coulomb interaction is considerably more complex than a constant interaction U, the latter provides a useful benchmark for assessing the robustness of the enhancement.

Finally, we turn to spectroscopic signatures of the enhanced superconducting state in order to identify experimentally accessible consequences beyond thermodynamic observables. In particular, we ask whether the emergence of the enhanced order gives rise to additional collective excitations.

To this end, we consider the operators

$$\mathfrak{A}_{\mathrm{Higgs}} = \frac{1}{\sqrt{N}} \sum_{\boldsymbol{k}} (\hat{c}^{\dagger}_{\boldsymbol{k},\uparrow} \hat{c}^{\dagger}_{-\boldsymbol{k},\downarrow} + \hat{c}_{-\boldsymbol{k},\downarrow} \hat{c}_{\boldsymbol{k},\uparrow}), \tag{7a}$$

$$\mathfrak{A}_{\mathrm{Phase}} = \frac{\mathrm{i}}{\sqrt{N}} \sum_{\boldsymbol{k}} (\hat{c}^{\dagger}_{\boldsymbol{k},\uparrow} \hat{c}^{\dagger}_{-\boldsymbol{k},\downarrow} - \hat{c}_{-\boldsymbol{k},\downarrow} \hat{c}_{\boldsymbol{k},\uparrow}), \tag{7b}$$

which are designed to excite Higgs modes or phase modes, respectively [26]. We evaluate the spectral functions $\mathcal{A}_{\alpha}(\omega) = -(1/\pi)\mathrm{Im}[\mathcal{G}_{\mathfrak{A}_{\alpha}\mathfrak{A}_{\alpha}^{\dagger}}(\omega)]$, with $\alpha \in \{\mathrm{Higgs}, \mathrm{Phase}\}$, at zero temperature via iterated equations of motion [26–30] truncated to bilinear operators. Diagrammatically, this approach is equivalent to solving the Bethe-Salpeter equation with bare mean-field propagators, including all interaction insertions while restricting the fermionic propagators to two lines.

Experimentally, collective phase and Higgs modes provide important spectroscopic fingerprints of superconductivity. While the phase mode can couple directly to external probes, the Higgs mode does not couple linearly to light [31]. Its observation therefore requires nonlinear driving, where the full Mexican-hat potential is excited [32–34]. These collective excitations thus offer a sensitive probe of the enhanced superconducting state.

Figure 4 shows the calculated spectral functions (a) $\mathcal{A}_{\mathrm{Higgs}}(\omega)$ and (b) $\mathcal{A}_{\mathrm{Phase}}(\omega)$ as a function of the interaction strength g. Collective excitations at finite energy appear mathematically as δ peaks and are therefore represented by Gaussian curves with identical spectral weight and an artificial broadening of $\sigma = 0.0005W$ for rendering purposes. The Goldstone mode associated with phase fluctuations is a δ' peak and is consequently shown as the derivative of a Gaussian. Since long-range Coulomb interaction is neglected, the Goldstone mode remains gapless; explicit calculations including this effect can be found, for example, in Ref. [11].

As expected, the spectra exhibit the well-established Higgs mode slightly below the quasiparticle continuum once the coupling becomes sufficiently strong. This mode was first reported by Barankov and Levitov [35] for a phenomenological momentum-dependent interaction and was later independently confirmed by Lorenzana and Seibold [10,36]. At still larger coupling strengths, additional secondary Higgs modes split off from the quasiparticle continuum, consistent with Ref. [11].

Most remarkably, however, is an emerging additional sharp collective mode, even inside the quasiparticle continuum. As the interaction strength increases, its energy decreases rapidly and eventually softens at $g = g_{\mathrm{enh}}$. Such a softening is a hallmark of an instability and naturally suggests that the onset of superconducting order around the DOS peak corresponds to a second superconducting condensation. In the framework of this interpretation, the soft mode is identified as the associated relative-phase (Leggett-like) excitation. The interpretation is corroborated by selectively probing the superconducting order localized around the DOS peak. Restricting the summation in the operators [Eq. (7b)] to the narrow energy window $|\varepsilon(\boldsymbol{k})| < 0.01W$ removes the conventional Higgs and phase responses from the spectra, leaving only the additional low-energy collective mode. The latter is therefore unambiguously associated with the enhanced superconductivity developing around ε_p.

The persistence of this mode inside the quasiparticle continuum is a consequence of the idealized model considered here. Since the enhanced and conventional superconducting orders remain energetically disconnected, the relative-phase mode couples only weakly to the quasiparticles near the Fermi energy. In contrast, the quasiparticles associated with the enhanced order reside at energies comparable to ε_p, allowing the mode to remain remarkably sharp despite lying inside the continuum. Furthermore, once the conventional and enhanced orders overlap, either by shifting E_{F} or by including additional interactions, the relative-phase mode broadens substantially.

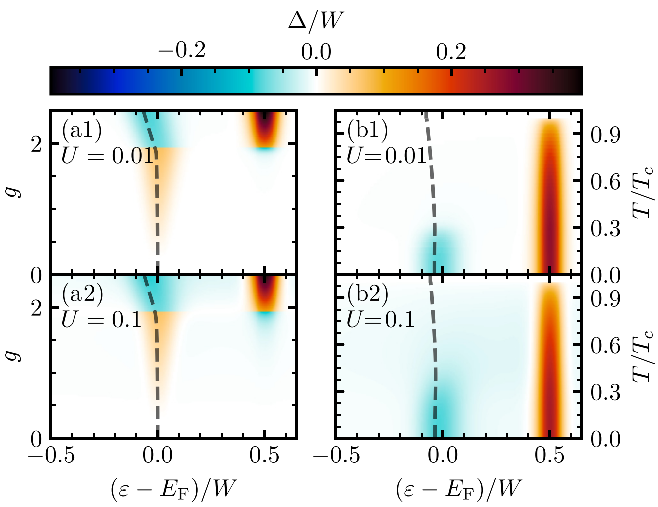

FIG. 5. (a) Calculated order parameter Δ at $T = 0$ as a function of the interaction strength g and the single-particle energy ε. The sign of Δ is chosen such that $\Delta(W) < 0$. The almost vertical dashed line marks the chemical potential μ. (b) Order parameter Δ as a function of the temperature T for $g = 2.2 > g_{\mathrm{enh}}$. The upper row (1) depicts the data for $U = 0.01$, while the lower row (2) depicts the data for $U = 0.1$. Note that the order parameter does not entirely vanish at the Fermi edge, but is severely reduced by higher temperatures. The enhanced contribution at the singularity of the DOS at $\varepsilon = \varepsilon_{\mathrm{peak}}$ remains the dominant contribution at larger T. At T_c, the system enters the normal phase. The order parameter exhibits no features beyond the ε range depicted in the plots.

IV. EFFECT OF A REPULSIVE INTERACTION

Here, we include the repulsive interaction and investigate how it modifies the superconducting order parameter. A repulsive interaction is expected to spread the order parameter over all energies and to induce a sign change [11,14,20,23–25]. Consequently, if the dominant contribution to Δ is positive, the order parameter becomes negative sufficiently far away in energy.

These expectations are confirmed in Fig. 5(a), which shows $\Delta(\varepsilon)$ as a function of the attractive interaction strength g and the energy ε. The upper row (1) corresponds to $U = 0.01$, while the lower row (2) displays the results for $U = 0.1$. In both cases, we exploit the global $U(1)$ symmetry to fix the overall phase of the order parameter by imposing the gauge condition $\Delta(W) < 0$. With this convention, the dominant superconducting contribution is immediately identified by its positive sign, irrespective of whether it is centered around the Fermi energy E_{F} or around the DOS peak at $\varepsilon = \varepsilon_{\mathrm{peak}}$.

As the repulsive interaction connects the conventional and enhanced superconducting orders, the threshold crossover coupling g_{enh} introduced for the idealized model ceases to be well defined once the two contributions overlap. While the sign change discussed above could be used to characterize the crossover, we find that a definition based on the behavior of the chemical potential is considerably more robust.

The temperature evolution of the order parameter is presented in Fig. 5(b) for $g = 2.2 > g_{\mathrm{enh}}$. For the weaker repulsion, $U = 0.01$, the behavior remains qualitatively similar to that of the idealized model, except that the conventional and enhanced contributions now have opposite signs. As the temperature increases, the conventional order around $\varepsilon \approx E_{\mathrm{F}}$ is suppressed much more rapidly than the enhanced order around $\varepsilon \approx \varepsilon_{\mathrm{peak}}$. In contrast to the idealized case, however, the order parameter at the chemical potential never vanishes completely. Consequently, the quasiparticle spectrum remains gapped throughout the superconducting phase. Increasing the repulsive interaction to $U = 0.1$ does not alter this picture qualitatively. The principal effect is that the order parameter acquires a larger magnitude away from the two dominant superconducting regions, reflecting the stronger coupling of the order parameters at different energies induced by the repulsive interaction.

Next, we study the evolution of the critical temperature T_c in Fig. 6. As before, the upper panel (a) depicts T_c, while the lower panel (b) displays the ratios $2\Delta_{\max}/T_c$ and $2\Delta_{\mathrm{true}}/T_c$. For reference, we also plot the data of Sec. III with $U = 0$ (blue lines). Importantly, the data for $U = 0$ and $U = 0.01$ (orange lines) almost match, indicating that the limit $U \to 0$ is captured by $U = 0$. For larger U (green and red lines), there are a few qualitative changes. The critical temperature does not increase as abruptly as before upon reaching g_{enh}. Nonetheless, an enhancement of T_c persists; it merely occurs more smoothly as a function of g. The larger U, the smoother T_c behaves.

The ratio $2\Delta_{\max}/T_c$ drops for $U = 0$ and $U = 0.01$ at $g \gtrsim g_{\mathrm{enh}}$. However, it rises for $U = 0.1$ and $U = 0.2$, even if g is slightly smaller than g_{enh}. In this region, $|\Delta(\varepsilon_{\mathrm{peak}})| > |\Delta(E_{\mathrm{F}})|$. Yet, the previously introduced condition $\Delta(W) < 0$ for the gauge entails $\Delta(E_{\mathrm{F}}) > 0$ and $\Delta(\varepsilon_{\mathrm{peak}}) < 0$. Thus, the

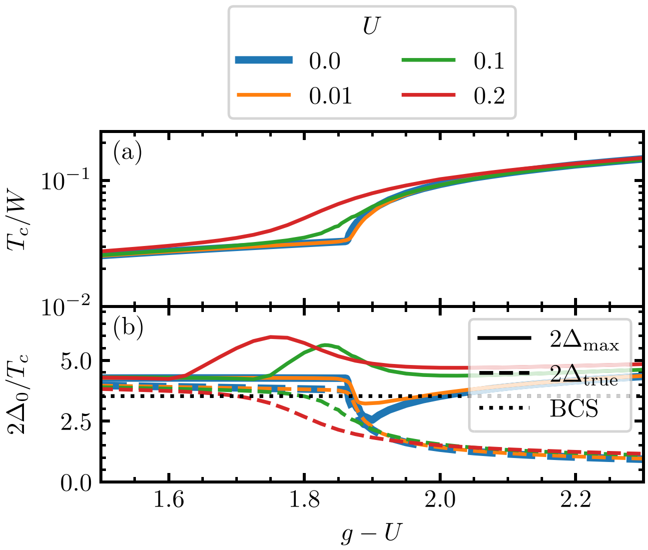

FIG. 6. Same as Fig. 16 except that we included the repulsive pseudopotential U. Additionally, we vary $g - U$ along the x axis and restrict the plot to the values of g near g_{enh}. The lines for $U = 0$ (blue) and $U = 0.01$ (orange) are almost identical.

conventional contribution at $\varepsilon \approx E_{\mathrm{F}}$ is still the dominant one. As T_c increases more quickly upon reaching g_{enh}, the ratio decreases again.

The ratio $2\Delta_{\mathrm{true}}/T_c$ behaves qualitatively the same in all considered cases. It decreases significantly for $g \gtrsim g_{\mathrm{enh}}$, although the decrease is slower the larger U is because T_c rises more slowly.

We next examine the thermodynamic signatures of the repulsive interaction through the specific heat C_V. Figure 7(a) shows C_V as a function of temperature for various coupling strengths g at $U = 0.01$. As before, the grayscale curves correspond to the conventional BCS-like regime ($g < g_{\mathrm{enh}}$), while the colored curves indicate the regime of enhanced superconductivity. Dashed lines denote the normal state above the critical temperature T_c.

For $g > g_{\mathrm{enh}}$, the additional low-temperature feature observed in the idealized model persists. Rather than a discontinuity, however, the specific heat exhibits a broadened hilltop when the conventional superconducting contribution becomes strongly suppressed, leaving only a small residual order parameter around the Fermi energy. The rounding of this anomaly originates from the repulsive interaction, which couples the conventional and enhanced superconducting orders over the entire energy range. Consequently, the enhanced order continues to induce a finite order parameter at $\varepsilon \approx E_{\mathrm{F}}$, preventing the sharp transition found for $U = 0$. The same mechanism also explains the broadening observed for large values of ω_{D}.

The corresponding results for the stronger repulsion, $U = 0.1$, are shown in Fig. 7(b). The qualitative behavior remains unchanged, but the low-temperature hilltop becomes substantially broader, reflecting the stronger coupling between the conventional and enhanced superconducting order parameters. For sufficiently large interaction strengths g, this feature is almost completely washed out, and the superconducting

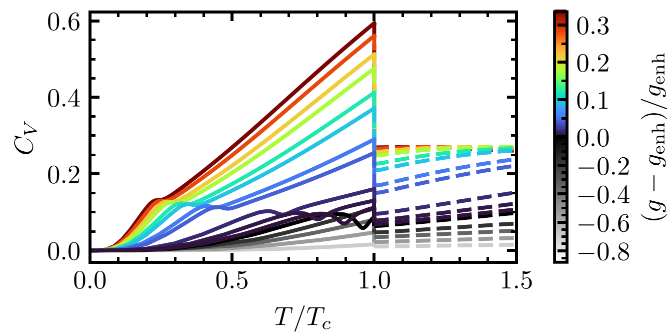

(a) $U = 0.01$, $g_{\mathrm{enh}} \approx 1.88$

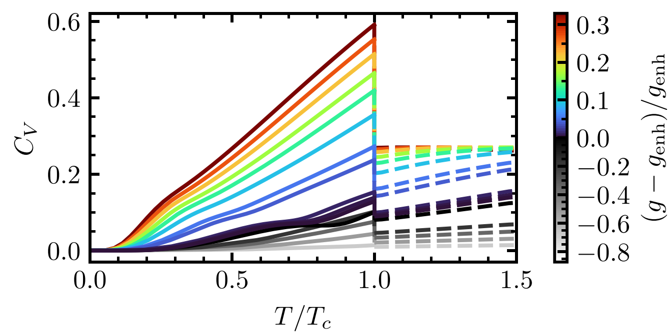

(b) $U = 0.1$, $g_{\mathrm{enh}} \approx 1.955$

FIG. 7. Same as Fig. 17 except that we included the repulsive effective potential U. We fixed $\omega_{\mathrm{D}} = 0.04W$ and set (a) $U = 0.01$ and (b) $U = 0.1$.

specific heat approaches an approximately linear temperature dependence.

Finally, we investigate the changes to the spectra of collective excitations induced by U. Figure 8 depicts the spectral functions $\mathcal{A}_\alpha(\omega) := (1/\pi)\mathcal{G}_\alpha(\omega)$, with (a) $\alpha =$ Higgs and (b) $\alpha =$ Phase. For the left column (1), we set $U = 0.01$. The global phase mode remains gapless at $\omega = 0$ because no proper long-range Coulomb interaction is included. The spectrum of secondary excitations, which was already presented

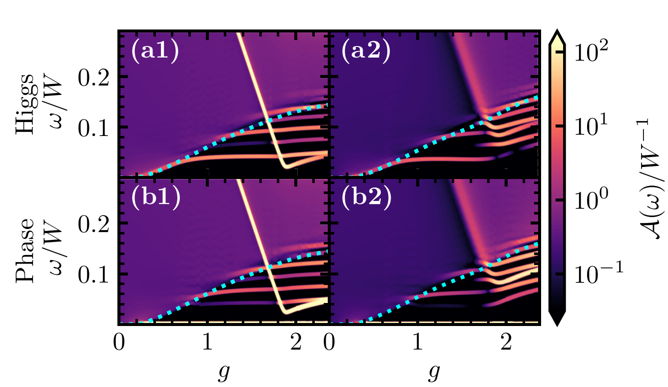

FIG. 8. Same as Fig. 20 except that now U is varied. The left panels (1) depict the data for $U = 0.01$, while the right panels (2) depict the data for $U = 0.1$. The secondary modes found in Ref. [11] are clearly visible. Additionally, another mode rapidly decreases in energy. Within the continuum, the mode is less dominant than in Fig. 4 and does not soften completely.

in Ref. [11], is largely unaffected by this small additional interaction.

The mode associated with the enhanced second SC order remains fairly sharp even within the quasiparticle continuum. However, it does not become completely soft for finite U. Instead, its energy reaches a minimum around $g \approx g_{\text{enh}}$ and then rises again.

In the right column (2), we set $U = 0.1$. The sharp collective mode has gained some width but remains clearly discernible as a prominent resonance. It emerges from the continuum at $g \approx 1.8$, but remains at these energies, i.e., does not soften.

This collective mode broadens whenever there is overlap between the conventional and enhanced contributions. If there is no overlap, the enhanced order does not directly couple to the conventional one. Moreover, the quasiparticle states corresponding to the enhanced order are energetically of the order of the Fermi level, i.e., exist at high energies. Thereby, in the idealized setting discussed in Sec. III, the collective mode couples directly only to these high-energy states, allowing it to remain sharp in the low-energy regime of the continuum. However, deviating from the idealized setting, as done here, induces such coupling and broadens the mode.

The results for finite local repulsion convey two messages. The first one is that the scenario of two consecutive phase transitions, one to conventional order, one to enhanced superconductivity, is too idealized due to the separation of energy scales. The second message, however, is that features of the two kinds of orderings, conventional and enhanced, persist and should be detectable. They appear less abrupt and more smeared out in comparison to the results at $U = 0$.

A valid point to raise is whether or not a small U is realistic. There are two possible responses to this question. First, one can compute the screened Coulomb potential via the standard random phase approximation

$$V_s(\omega, \boldsymbol{q}) = \frac{V(\boldsymbol{q})}{1 + \chi_0(\omega, \boldsymbol{q})V(\boldsymbol{q})}, \tag{8}$$

with the Lindhard function

$$\chi_0(\omega, \boldsymbol{q}) = 2\sum_{\boldsymbol{k}} \frac{f(\varepsilon_{\boldsymbol{k}+\boldsymbol{q}}) - f(\varepsilon_{\boldsymbol{k}})}{\omega + \varepsilon_{\boldsymbol{k}} - \varepsilon_{\boldsymbol{k}+\boldsymbol{q}}} \tag{9}$$

and the unscreened Coulomb potential [37]

$$V(\boldsymbol{q}) = \frac{1}{N\mathcal{V}} \frac{e^2}{\epsilon_0 q^2}. \tag{10}$$

Here, $f(\varepsilon)$ is the Fermi function, N the number of lattice sites, $\mathcal{V}$ the volume of the unit cell, e the elementary charge, and ϵ_0 the vacuum permittivity. The physics for finite ω are very rich, since there can be resonances in $V_s(\omega, \boldsymbol{q})$, where the Coulomb interaction becomes overscreened and *constructive* interference can occur. These rich dynamical effects are beyond the scope of the present work and are left for future studies. Instead, we compute the average of the screened potential over the first Brillouin zone

$$U_s(\omega) := \rho_{\text{F}} \sum_{\boldsymbol{q} \in 1^{\text{st}}\text{BZ}} V_s(\omega, \boldsymbol{q}) \tag{11}$$

and take it as an estimate for the pseudopotential U because the Coulombic repulsion is strongest at small $\boldsymbol{q}$ values,

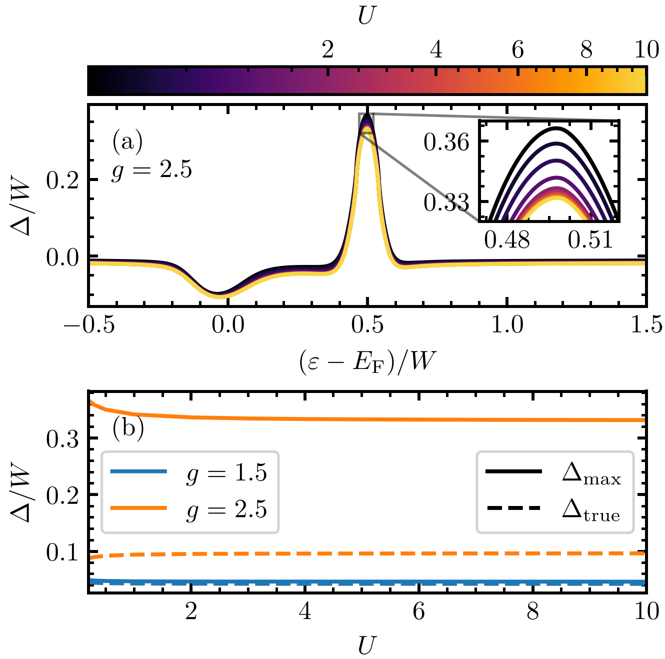

FIG. 9. (a) Self-consistently computed order parameter Δ for $0.2 \leqslant U \leqslant 10$ and $g = 2.5$. The colors correspond to the different values of U. (b) Maximum of the order parameter Δ_{max} (solid lines) and the system's actual energy gap Δ_{true} (dashed lines) as a function of U for $g = 1.5 < g_{\text{enh}}$ (blue) and $g = 2.5 > g_{\text{enh}}$ (orange).

whereas the effective electron-electron interaction is attractive over almost the entire Brillouin zone as long as the energy difference is smaller than ω_{D}. Hence, only the momentum average of the Coulombic repulsion is relevant to assess whether the attractive interaction is overturned. Since our pairing only occurs up to ω_{D}, we only care about small values of ω in the order of ω_{D}. Recall that the enhanced and conventional orders are not connected via the pairing potential. Then, choosing lattice constants on the order of a few Ångströms and W on the order of a few electronvolts, the calculation yields $0.3 \lessapprox U_s(\omega) \lessapprox 0.5$. In the relevant region $\omega \lessapprox \omega_{\text{D}}$, the average is largely independent of the precise choice of ω. Hence, we omit the frequency dependence of $U_s(\omega)$ and work with a constant repulsion U.

To see how sensitive the results are to larger values of U, we show that no further qualitative changes appear upon increasing U, even if its value is increased beyond g. Figure 9 shows (a) the order parameter for $0.2 \leqslant U \leqslant 10$ and $g = 2.5$ and (b) its maximum Δ_{max} and the system's actual energy gap Δ_{true} as a function of U for $g = 1.5 < g_{\text{enh}}$ and $g = 2.5 > g_{\text{enh}}$. Importantly, the quantities remain largely unaffected, even quantitatively, by large U. Morel and Anderson showed that in their model, the effective repulsion becomes [20]

$$\mu^* = \frac{U}{1 + U\ln(E_{\text{F}}/\omega_{\text{D}})}. \tag{12}$$

Thus, in the limit $U \to \infty$, one finds $\mu^* = 1/\ln(E_{\text{F}}/\omega_{\text{D}})$, independent of U. Of course, the present model is different from that of Morel and Anderson. Nevertheless, the above

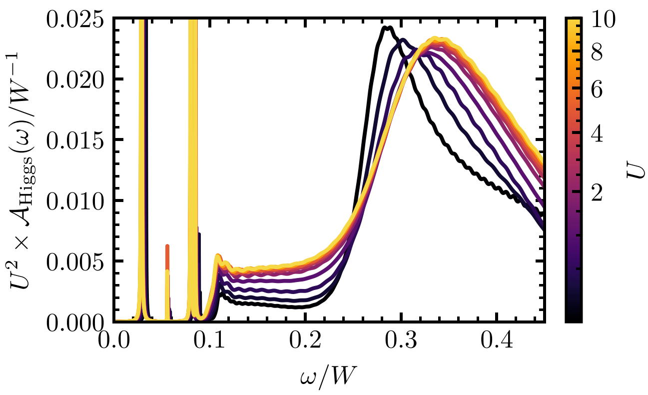

FIG. 10. Amplitude spectral function $\mathcal{A}_{\mathrm{Higgs}}(\omega)$ scaled by U^2 for $0.2 \leqslant U \leqslant 10$ and $g = 1.5$. The colors correspond to the various values of U as indicated by the legend on the right-hand side. Outside of the continuum, the frequencies are shifted into the complex plane $\omega \to \omega + 10^{-4}\mathrm{i}W$ to broaden the subgap excitations for visualization.

results suggest that a similar mechanism is at play and that the effective repulsion stays moderate.

The contribution to the order parameter induced by U is given by

$$\Delta_U = -\frac{U}{\tilde{\rho}} \int_{-W}^{W} \rho(\varepsilon) \frac{\Delta(\varepsilon)}{2E(\varepsilon)}. \tag{13}$$

This integral is strongly suppressed by the sign change of the order parameter as a function of energy, which causes the sum to contain nearly equal positive and negative contributions. Thus, the sign change allows the system to circumvent the repulsion optimally [23]. There is also no notable change in the other mean-field quantities, such as T_c, since they, in effect, depend on Δ. Therefore, we do not show additional plots of their dependencies.

Figure 10 shows the amplitude spectral function $\mathcal{A}_{\mathrm{Higgs}}(\omega)$ for the range $0.2 \leqslant U \leqslant 10$. Here, we focus on the mode appearing inside the continuum, and therefore set $g = 1.5 < g_{\mathrm{enh}}$. We notice that the spectral functions generally diminish in magnitude as U increases. To improve visibility, each line in the figure is therefore multiplied by U^2, which largely removes the scaling effects. Aside from this overall scaling, however, there is little change in the spectral functions across different values of U. The resonance shifts slightly but appears to have converged for $U = 10$. Its weight relative to the remainder of the spectral function is also largely unaffected by changing U.

All in all, these results provide evidence that the advocated enhanced superconductivity is robust even upon inclusion of Coulomb repulsion, even unscreened.

V. THE QUASIPARTICLE DENSITY OF STATES

Finally, we discuss a few examples of the quasiparticle densities of states (QP-DOS) defined by [38]

$$\rho_{\mathrm{qp}}(E) = \int_{-W}^{W} \mathrm{d}\varepsilon\, \rho(\varepsilon) \big[u_\varepsilon^2 \delta(E - E(\varepsilon)) + v_\varepsilon^2 \delta(E + E(\varepsilon))\big], \tag{14}$$

with the coherence factors

$$u_\varepsilon^2 = \frac{1}{2}\left(1 + \frac{\varepsilon - \mu}{E(\varepsilon)}\right), \quad v_\varepsilon^2 = \frac{1}{2}\left(1 - \frac{\varepsilon - \mu}{E(\varepsilon)}\right). \tag{15}$$

This quantity can be readily measured experimentally, for instance via tunneling spectroscopy [39].

Figure 11 shows the QP-DOS for the parameters chosen in Sec. III $\omega_{\mathrm{D}} = 0.04W$, $E_{\mathrm{F}} = -0.5W$, and $U = 0$. In panel (a), $g = 1 < g_{\mathrm{enh}}$. Consequently, we find mostly BCS behavior, notwithstanding a slight asymmetry of the coherence peaks at $E = \pm\Delta_{\mathrm{true}}$. We attribute this asymmetry to the electronic DOS itself. In addition to the coherence peaks and the energy gap, we observe the underlying DOS of the bcc system at all temperatures.

In panel (b), $g = 2 > g_{\mathrm{enh}}$. Here, we again observe the energy gap and asymmetric coherence peaks at sufficiently low temperatures. As discussed in Sec. III, the gap vanishes at higher T before the enhanced SC order disappears. Concurrently, the coherence peaks also disappear. However, we do not advocate gapless SC since other couplings, e.g., U, extend the order parameter over the entire parameter space.

Interestingly, the logarithmic singularity of the electronic DOS acquires additional structure as the enhanced order sets in around it. This manifests in a dip followed by a rapid increase in the QP-DOS. Simultaneously, the QP-DOS acquires substantial weight and another peak for $E < -\sqrt{(-W - \mu)^2 + \Delta^2(-W)}$. This weight appears around $E \approx -\sqrt{(\varepsilon_{\mathrm{peak}} - \mu)^2 + \Delta^2(\varepsilon_{\mathrm{peak}})}$. Thus, it is a mirrored effect of the structure at positive E due to the presence of the enhanced order.

In panel (c), we increase $g = 2.5$. We observe the same features as in panel (b), but more pronounced.

Figure 12 is analogous to Fig. 11, except that we set $E_{\mathrm{F}} = -0.2W$. For $g = 1 < g_{\mathrm{enh}}$ [panel (a)], we again observe mainly BCS behavior. The aforementioned asymmetry of the coherence peaks is more pronounced here, which we attribute to the steeper bare electronic DOS.

For $g > g_{\mathrm{enh}}$ [panels (b)–(c)], we find a similar new structure around the previous logarithmic peak of the electronic DOS. Additionally, a mirrored structure, including corresponding peaks, manifests at $E \approx -\sqrt{(\varepsilon_{\mathrm{peak}} - \mu)^2 + \Delta^2(\varepsilon_{\mathrm{peak}})}$. This result clearly shows that this structure and the enhanced SC order are closely linked.

Last, we show the QP-DOS for $U = 0.1$ in Fig. 13. As before, in panel (a) with $g = 1 < g_{\mathrm{enh}}$, we observe mainly BCS behavior, except for the aforementioned slight asymmetry of the coherence peaks.

The behavior in panels (b) and (c) is qualitatively the same as in Fig. 11, except that, as discussed before, the energy gap never truly vanishes for $T < T_c$. For clarification, we additionally provide a plot of the QP-DOS enlarged around the energy gap in Fig. 14. In panel (a), we set $U = 0$, causing the energy gap to be exponentially suppressed, which appears as 0 in the numerics and in the plot, for sufficiently large T. This does not happen in panel (b) with $U = 0.1$. Other than that, we still observe the additional structure around the logarithmic singularity of the electronic DOS and at $E \approx -\sqrt{(\varepsilon_{\mathrm{peak}} - \mu)^2 + \Delta^2(\varepsilon_{\mathrm{peak}})}$.

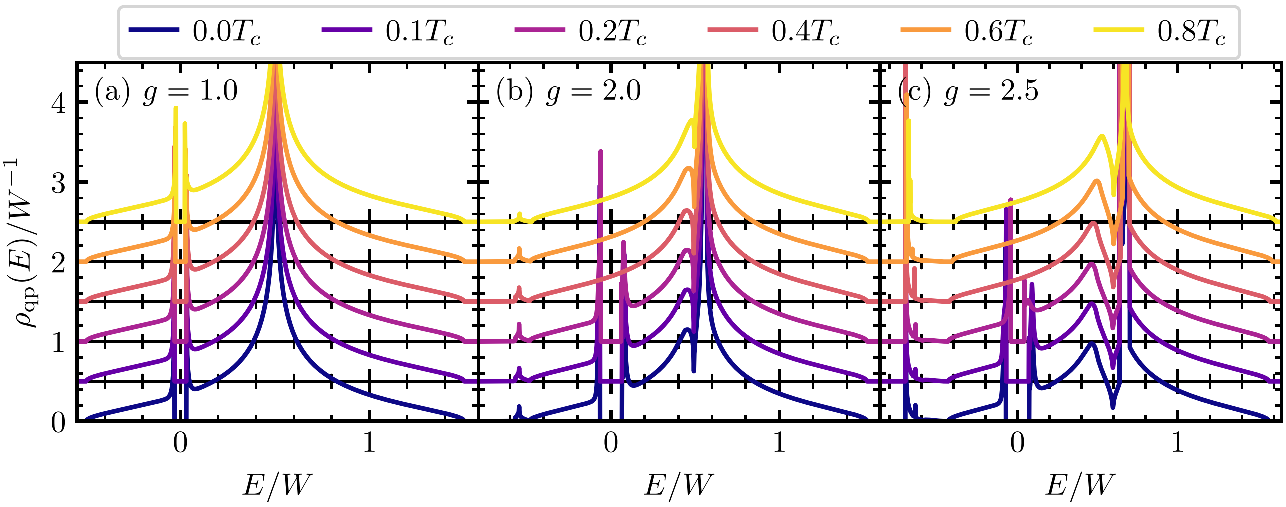

FIG. 11. Calculated quasiparticle density of states (14) for $\omega_{\rm D} = 0.04W$, $E_{\rm F} = -0.5W$, and $U = 0$. The individual panels (a)–(c) show the data for $g = 1,\ 2,\ 2.5$. Enhanced superconductivity occurs in panels (b) and (c). The different colors represent different temperatures in units of T_c as given in the legend. The lines are shifted by 0.5 with respect to each other to improve visibility.

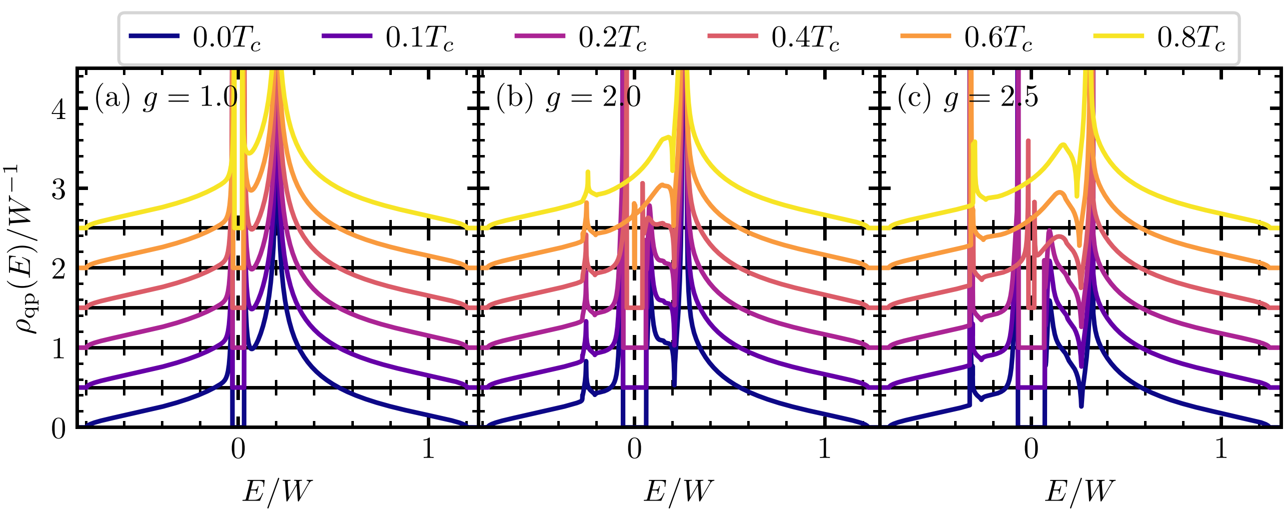

FIG. 12. Same as Fig. 11 except that $E_{\rm F} = -0.2W$.

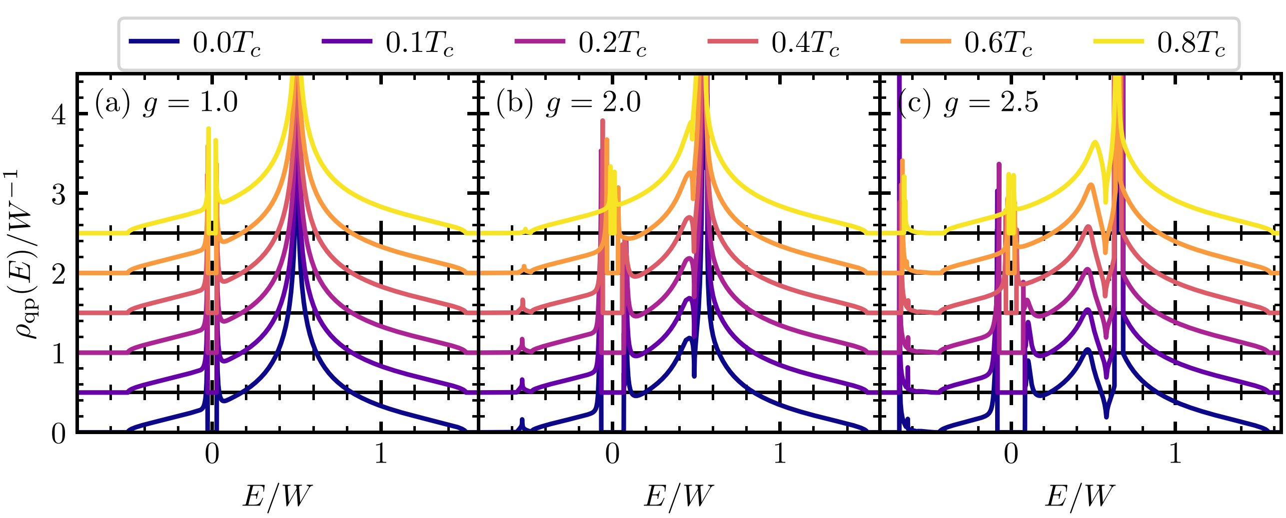

FIG. 13. Same as Fig. 11 except that $U = 0.1$.

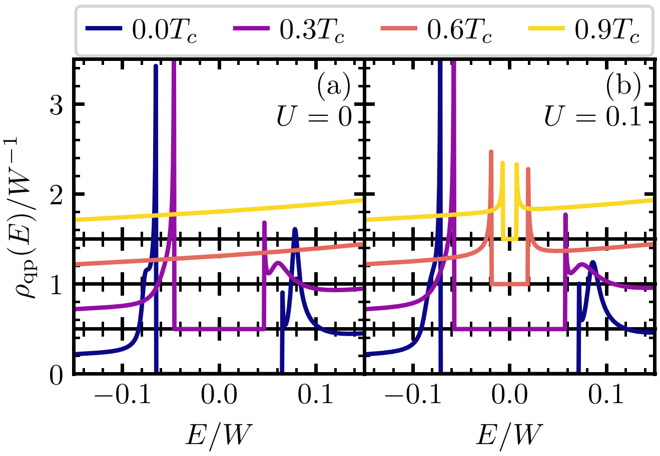

FIG. 14. QP-DOS for $g - U = 2$, $E_F = -0.5W$ enlarged around the energy gap. We set (a) $U = 0$ and (b) $U = 0.1$.

In conclusion, these additional features are robust against the inclusion of additional repulsive interactions. Thereby, we are able to predict an additional quantity that is readily accessible in experiments.

VI. CONCLUSION

In conclusion, we have shown that a pronounced peak in the density of states can stabilize a dominant superconducting order parameter at an energy ε_p away from the Fermi level. Remarkably, this enhancement occurs even if the DOS peak lies outside the phonon window around the Fermi energy, i.e., for $|E_F - \varepsilon_p| > \omega_D$. It therefore originates from the full energy-transfer dependence of the electron-phonon interaction and is absent within the conventional BCS approximation.

The emergence of this enhanced superconducting order has profound consequences for the physical properties of the system. Above a threshold interaction strength g_{enh}, the critical temperature increases dramatically, while the quasiparticle gap remains governed by the conventional superconducting order, resulting in an unusually small ratio $2\Delta_{\text{true}}/T_c$. The crossover is accompanied by characteristic thermodynamic and spectroscopic signatures. In particular, the specific heat develops an additional anomaly associated with the suppression of the conventional order, and an additional collective relative-phase mode softens at the onset of the enhanced superconducting state. Together, these features provide experimentally accessible fingerprints of enhanced superconductivity away from the Fermi level.

To assess the robustness of these predictions, we included a phenomenological Hubbard-like repulsive interaction. While the additional repulsion smooths the thermodynamic anomalies and broadens the spectral resonance of the collective mode, the enhanced superconducting order itself persists even for comparatively strong repulsion. These findings indicate that the phenomenon is not an artifact of the idealized model but a robust consequence of the energy dependence of the pairing interaction.

The constant repulsive interaction employed here is, of course, only a phenomenological approximation. A quantitative description requires the dynamically screened Coulomb interaction [37], whose momentum and frequency dependence gives rise to substantially richer physics. In particular, poles of $\chi(\omega, \mathbf{q})$ correspond to plasmon excitations, for which the screened Coulomb interaction can become overscreened and even attractive in parts of momentum and frequency space [40–42]. Such plasmon-mediated pairing may interfere constructively with the phonon-mediated mechanism considered here, especially at energies away from the Fermi level where the enhanced superconducting order develops. Exploring this interplay constitutes an intriguing direction for future work. Nevertheless, within the spirit of the Anderson-Morel pseudopotential, the momentum- and frequency-averaged screened Coulomb interaction is expected to remain repulsive overall. In this sense, the phenomenological interaction U employed here provides a meaningful first step toward assessing the robustness of the proposed mechanism.

Our work thus identifies a previously unexplored route toward enhancing superconductivity beyond the conventional BCS paradigm. We hope that the predicted thermodynamic and spectroscopic signatures will stimulate both experimental searches and microscopic theoretical studies of superconductivity away from the Fermi level.

ACKNOWLEDGMENTS

We acknowledge constructive discussions with D. Hering, V. Sulaimann, S. Behrensmeier, and J. Stolze. This research was partially funded by the MERCUR Kooperation through Project No. KO-2021-0027.

DATA AVAILABILITY

The data that support the findings of this article are openly available [43].

APPENDIX A: DERIVATION OF THE EFFECTIVE ELECTRON-ELECTRON INTERACTION

Here, we derive the effective electron-electron interaction, following the original ideas in Ref. [17]. We begin with a Hamiltonian including one phonon branch and the electron-phonon coupling

$$\begin{aligned}\mathcal{H} = &\sum_{\boldsymbol{k}}\sum_{\sigma}\varepsilon_{\boldsymbol{k}}\hat{c}^\dagger_{\boldsymbol{k},\sigma}\hat{c}_{\boldsymbol{k},\sigma} + \sum_{\boldsymbol{q}}\omega_{\boldsymbol{q}}\hat{b}^\dagger_{\boldsymbol{q}}\hat{b}_{\boldsymbol{q}} \\ &+ \sum_{\boldsymbol{kq}}\sum_{\sigma}(M_{\boldsymbol{k},\boldsymbol{q}}\hat{b}^\dagger_{-\boldsymbol{q}}\hat{c}^\dagger_{\boldsymbol{k}+\boldsymbol{q},\sigma}\hat{c}_{\boldsymbol{k},\sigma} + \text{H.c.}) \\ &+ \sum_{\boldsymbol{kk'q}}\sum_{\sigma\sigma'}V^{\text{eff}}_{\boldsymbol{k},\boldsymbol{k'},\boldsymbol{q}}\hat{c}^\dagger_{\boldsymbol{k}+\boldsymbol{q},\sigma}\hat{c}^\dagger_{\boldsymbol{k'}-\boldsymbol{q},\sigma'}\hat{c}_{\boldsymbol{k'},\sigma'}\hat{c}_{\boldsymbol{k},\sigma}. \end{aligned} \tag{A1}$$

Here, $\hat{b}^{(\dagger)}_{\boldsymbol{q}}$ annihilates (creates) a phonon with momentum $\boldsymbol{q}$. The phonon dispersion is $\omega_{\boldsymbol{q}}$, and the electron-phonon coupling is $M_{\boldsymbol{k},\boldsymbol{q}}$. Initially, $M_{\boldsymbol{k},\boldsymbol{q}} \equiv M_{\boldsymbol{q}}$ is independent of the electron's momentum, but it will acquire such a dependence during the calculations. Similarly, the effective electron-electron interaction $V^{\text{eff}}_{\boldsymbol{k},\boldsymbol{k'},\boldsymbol{q}}$ initially vanishes identically, but becomes finite as the subsystems are decoupled. We assume inversion symmetry $\varepsilon_{\boldsymbol{k}} = \varepsilon_{-\boldsymbol{k}}$ and $\omega_{\boldsymbol{q}} = \omega_{-\boldsymbol{q}}$. The normalization constant $1/\sqrt{N}$ is absorbed in $M_{\boldsymbol{k},\boldsymbol{q}}$.

We decouple the electronic and phononic degrees of freedom by employing a continuous unitary transformation [13,15,17]. To this end, one needs to solve the flow equation

$$\partial_\ell \mathcal{H}(\ell) = [\eta(\ell), \mathcal{H}(\ell)]. \tag{A2}$$

The flow is initialized at $\ell = 0$ with Eq. (A1). For $\ell \to \infty$, we obtain the effective, decoupled Hamiltonian.

The decoupling is achieved by employing the generator [17]

$$\eta(\ell) = \sum_{kq}\sum_{\sigma} \mathrm{sgn}[\alpha(\boldsymbol{k},\boldsymbol{q})] M_{\boldsymbol{k},\boldsymbol{q}}(\ell)\hat{b}^{\dagger}_{-\boldsymbol{q}}\hat{c}^{\dagger}_{\boldsymbol{k}+\boldsymbol{q},\sigma}\hat{c}_{\boldsymbol{k},\sigma} + \sum_{kq}\sum_{\sigma} \mathrm{sgn}[\beta(\boldsymbol{k},\boldsymbol{q})] M^{*}_{\boldsymbol{k}+\boldsymbol{q},-\boldsymbol{q}}(\ell)\hat{b}_{\boldsymbol{q}}\hat{c}^{\dagger}_{\boldsymbol{k}+\boldsymbol{q},\sigma}\hat{c}_{\boldsymbol{k},\sigma} \tag{A3}$$

in leading order in M with the abbreviations

$$\alpha(\boldsymbol{k},\boldsymbol{q}) = \varepsilon_{\boldsymbol{k}+\boldsymbol{q}}(\ell) - \varepsilon_{\boldsymbol{k}}(\ell) + \omega_{\boldsymbol{q}}(\ell), \tag{A4a}$$

$$\beta(\boldsymbol{k},\boldsymbol{q}) = \varepsilon_{\boldsymbol{k}+\boldsymbol{q}}(\ell) - \varepsilon_{\boldsymbol{k}}(\ell) - \omega_{\boldsymbol{q}}(\ell) = -\alpha(\boldsymbol{k}+\boldsymbol{q},-\boldsymbol{q}). \tag{A4b}$$

This generator does not extend the virtual processes beyond $|\varepsilon_{\boldsymbol{k}+\boldsymbol{q}} - \varepsilon_{\boldsymbol{k}}| \leqslant \omega_{\boldsymbol{q}}$ [44–46].

We are only interested in the effective electron-electron interaction in second order in M and drop higher-order contributions. This procedure yields the flow equation for the electron-phonon coupling

$$\partial_\ell M_{\boldsymbol{k},\boldsymbol{q}}(\ell) = -|\alpha(\boldsymbol{k},\boldsymbol{q})| M_{\boldsymbol{k},\boldsymbol{q}}(\ell) \tag{A5a}$$

$$\Rightarrow M_{\boldsymbol{k},\boldsymbol{q}}(\ell) = M_{\boldsymbol{q}} e^{-|\alpha(\boldsymbol{k},\boldsymbol{q})|\ell} + \mathcal{O}(M^3). \tag{A5b}$$

The solution is exact in $\mathcal{O}(M^2)$ because the electronic dispersion $\varepsilon_{\boldsymbol{k}}$ becomes ℓ dependent only in $\mathcal{O}(M^2)$. Notably, the electron-phonon coupling is eliminated for $\ell \to \infty$, unless $\alpha(\boldsymbol{k},\boldsymbol{q}) = 0$. However, these specific points in a six-dimensional parameter space, spanned by $\boldsymbol{k}$ and $\boldsymbol{q}$, form a set of measure zero and may be ignored.

Using Eq. (A5b), the effective electron-electron interaction is expressed as

$$\partial_\ell V^{\mathrm{eff}}_{\boldsymbol{k},\boldsymbol{k}',\boldsymbol{q}}(\ell) = [\mathrm{sgn}[\beta(\boldsymbol{k}',-\boldsymbol{q})] - \mathrm{sgn}[\alpha(\boldsymbol{k},\boldsymbol{q})]]|M_{\boldsymbol{q}}|^2 \exp[-(|\alpha(\boldsymbol{k},\boldsymbol{q})| + |\alpha(\boldsymbol{k}'-\boldsymbol{q},\boldsymbol{q})|)\ell] \tag{A6a}$$

$$\Rightarrow V^{\mathrm{eff}}_{\boldsymbol{k},\boldsymbol{k}',\boldsymbol{q}}(\infty) = |M_{\boldsymbol{q}}|^2 \left[\frac{\mathrm{sgn}[\alpha(\boldsymbol{k},\boldsymbol{q})] - \mathrm{sgn}[\beta(\boldsymbol{k}',-\boldsymbol{q})]}{|\alpha(\boldsymbol{k},\boldsymbol{q})| + |\beta(\boldsymbol{k}',-\boldsymbol{q})|}\right]. \tag{A6b}$$

As before, this result is exact in second order in M. Notably, this perturbative expansion is the only approximation made to arrive at this result. As we chiefly care about superconductivity and not about renormalizations of the single-particle dispersion, we extract the BCS channel

$$g(\boldsymbol{k},\boldsymbol{k}') := V^{\mathrm{eff}}_{\boldsymbol{k},\boldsymbol{k}',\boldsymbol{q}} = -\frac{|M_{\boldsymbol{k}'-\boldsymbol{k}}|^2}{\omega_{\boldsymbol{k}'-\boldsymbol{k}}}\Theta(\omega_{\boldsymbol{k}'-\boldsymbol{k}} - |\varepsilon_{\boldsymbol{k}} - \varepsilon'_{\boldsymbol{k}}|). \tag{A7}$$

Choosing $|M_{\boldsymbol{k}'-\boldsymbol{k}}|^2 = \mathrm{const}$ and $\omega_{\boldsymbol{k}'-\boldsymbol{k}} = \omega_{\mathrm{D}} = \mathrm{const}$ yields Eq. (2).

Note that this interaction is always attractive, and the interaction is cut off sharply if $|\varepsilon_{\boldsymbol{k}} - \varepsilon'_{\boldsymbol{k}}| > \omega_{\boldsymbol{k}'-\boldsymbol{k}}$. In general, this does not need to be the case as unitary transformations that achieve such a decoupling are not uniquely determined [16,17]. For example, in his foundational work, Fröhlich provided a result that is only attractive for momenta close to the Fermi level [12]. Moreover, a result similar to ours was derived by Lenz and Wegner [13]. While their result is also always attractive, the interaction strength merely decreases as a power law in $|\varepsilon_{\boldsymbol{k}} - \varepsilon_{\boldsymbol{k}'}|^{-2}$. These comparisons, also presented in Ref. [17], highlight the advantages of the calculations described here.

APPENDIX B: THE CHEMICAL POTENTIAL

As mentioned in the main text, we fix the filling n to the filling of the would-be normal state with $\mu = E_{\mathrm{F}}$ at $T = 0$, i.e.

$$n = 2\int_{-W}^{E_{\mathrm{F}}} \mathrm{d}\varepsilon\, \rho(\varepsilon), \tag{B1}$$

where the factor of 2 refers to the spin degeneracy. Requiring this filling to remain constant implicitly defines the chemical potential μ as a function of both g and T.

Figure 15 shows plots of $\mu(T) - E_{\mathrm{F}}$ for various g. Note that this shift remains rather small in all considered cases. The dotted line is the chemical potential of the would-be normal state. The thick lines represent the first line shown with

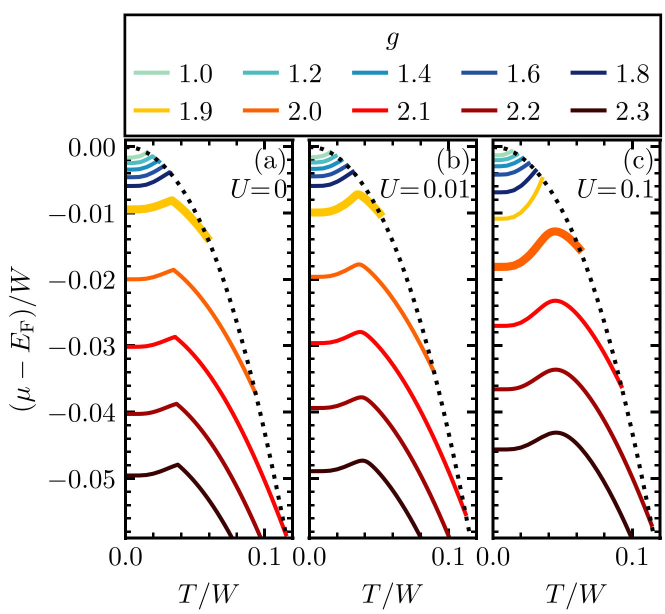

FIG. 15. Calculated chemical potential shift relative to E_{F} as a function of the temperature T for various interaction strengths g. The dotted line is the chemical potential of the would-be normal state. The individual panels (a)–(c) use different local repulsions U. The thick line in each panel marks the first line with $g > g_{\mathrm{enh}}$.

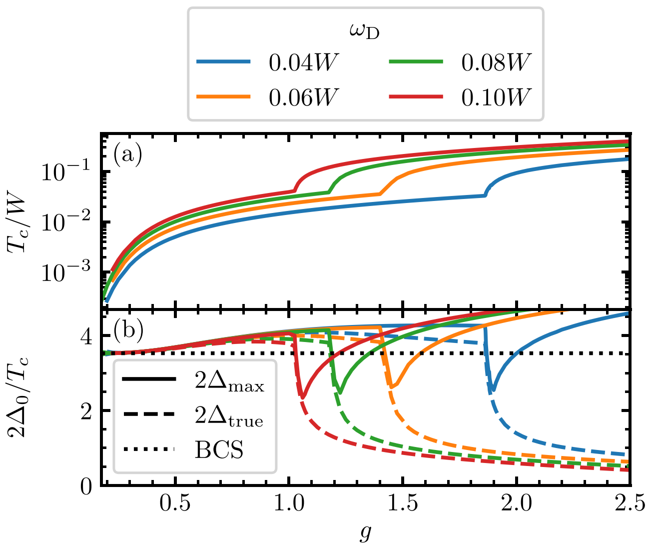

FIG. 16. (a) Calculated critical temperature T_c as a function of the interaction strength g. The y axis is scaled logarithmically. (b) Ratio of the maximum value of the order parameter Δ_{max} (solid lines) and energy gap of the quasiparticle dispersion Δ_{true} (dashed lines) at $T = 0$ to T_c as a function of the interaction strength g. The black dotted line marks the BCS ratio (≈3.528) [22].

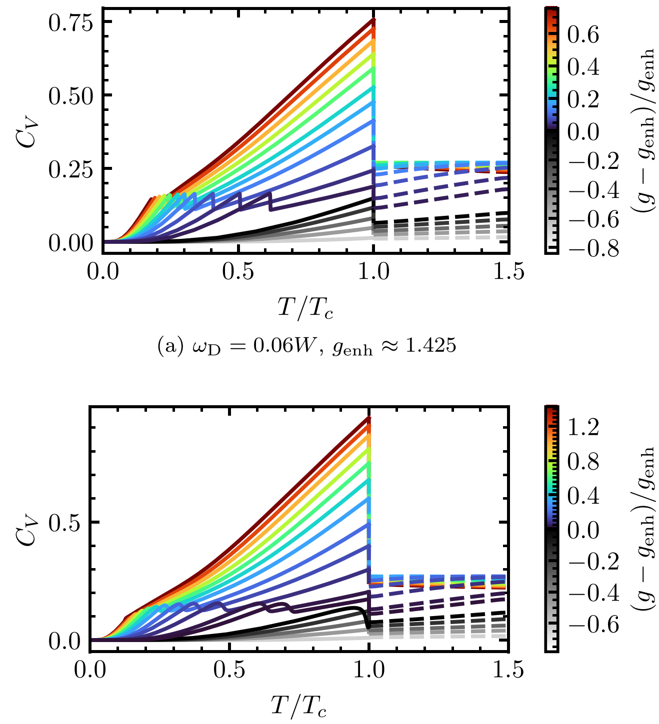

(a) $\omega_D = 0.06W$, $g_{enh} \approx 1.425$

(b) $\omega_D = 0.1W$, $g_{enh} \approx 1.03$

FIG. 17. Calculated specific heat C_V as a function of the temperature T. We used (a) $\omega_D = 0.06W$ and (b) $\omega_D = 0.08W$. The different colors indicate different coupling strengths g as indicated by the legend. The solid lines indicate the superconducting state, while the dashed lines indicate the normal state. For $g < g_{enh}$ (in grayscale), we observe renormalized BCS behavior. For $g > g_{enh}$ (colored), we find qualitatively unexpected behavior due to the enhanced SC away from E_F.

$g > g_{enh}$. We used the same parameters as in the main text for panel (a). For panels (b) and (c), we additionally considered the local Hubbard-like repulsion U.

In any case, as expected, the μ of the superconducting system approaches the μ of the normal state system for $T \to T_c$. If $g < g_{enh}$, the chemical potential rises slightly as $T \to T_c$. For $g > g_{enh}$, $\mu(T)$ reaches a maximum and then rapidly decreases until reaching T_c.

The existence of such a maximum provides a more robust definition of g_{enh}: g_{enh} is the first g, at which $\mu(T)$ exhibits a local maximum. This definition works even if the conventional and enhanced contributions overlap and is used throughout this work. At least in all considered cases, this definition yields the g at which the ratio $2\Delta_{true}/T_c$ decreases the fastest. Thus, choosing the g of the steepest descent of this ratio provides an equivalent definition.

APPENDIX C: EFFECT OF THE DEBYE FREQUENCY

We begin by studying the effect of varying ω_D. In Fig. 16(a), we plot T_c as a function of the interaction strength g. The blue curve is the same as in the main text with $\omega_D = 0.04W$. The three other curves correspond to different ω_D. Notably, the same enhancement of T_c exists for all depicted cases. The only difference is the crossover interaction g_{enh} at which this phenomenon occurs. Generally, a larger Debye frequency, or equivalently, a smaller electronic bandwidth $2W$, causes the enhancement to set in at smaller values of g.

In Fig. 16(b), we plot the maximum of the order parameter Δ_{max} (solid lines) and the energy gap Δ_{true} (dashed lines) in units of T_c. The dotted line marks the BCS ratio ≈3.528 [22]. We find the same behavior in all cases. In the weak-coupling regime, we recover the BCS prediction. For intermediate coupling, we observe that $\Delta_{true} < \Delta_{max}$, due to the shift of the minimum of the quasiparticle dispersion (cf. Ref. [11]). Around $g = g_{enh}$, the ratios plummet and only Δ_{max}/T_c recovers. The analysis of this feature is the same as the one provided in the main text.

In Fig. 17, we plot the specific heat as a function of temperature with (a) $\omega_D = 0.06W$ and (b) $\omega_D = 0.08W$. The solid lines mark $T < T_c$, while the dashed lines mark $T > T_c$. The grayscale lines represent $g < g_{enh}$, in which case we qualitatively find the BCS behavior. The colored lines mark $g > g_{enh}$. Here, we initially observe the same feature as in the main text: The conventional contribution at $\Delta(E_F)$ vanishes before the enhanced contribution $\Delta(\varepsilon_{peak})$ does. This induces an additional discontinuity in C_V before the system enters the normal phase. However, as g increases further, the conventional and enhanced contributions overlap. Then, the aforementioned discontinuity smears out. This behavior is clearly noticeable for large g in Fig. 17(b).

APPENDIX D: EFFECT OF THE FERMI ENERGY

Next, we perform the same analysis as in the previous section but for the Fermi energy E_F. Figure 18(a) depicts T_c as a function of g. If E_F is sufficiently far away from the logarithmic divergence of the DOS at $\varepsilon = \varepsilon_{peak} = 0$, we find the same behavior as described in the main text: The critical

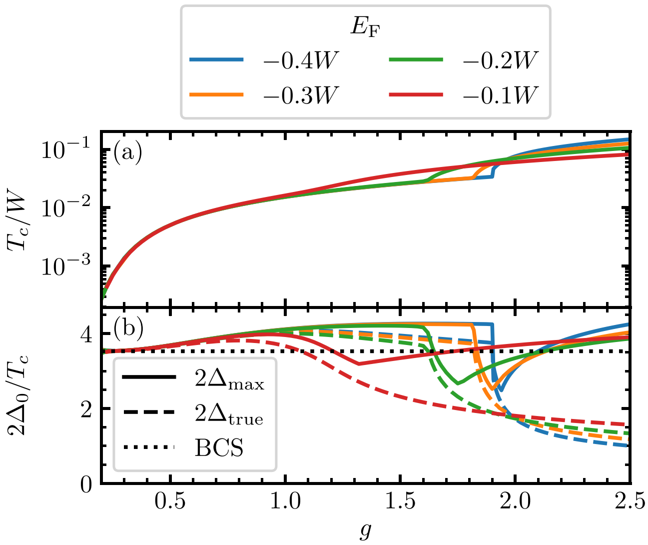

FIG. 18. Same as Fig. 16 except that E_F is varied.

temperatures significantly increase upon passing the threshold g_{enh}. However, this enhancement weakens as the Fermi energy approaches 0. For $E_F = -0.1W$, the enhancement is barely noticeable anymore. This behavior occurs because the contributions of $\Delta(E_F)$ and $\Delta(\varepsilon_{peak})$ merge as $E_F \to 0$. Thus, it becomes impossible to distinguish between an enhanced and a conventional contribution.

The ratios of the energy gap $2\Delta_{true}$ and of the maximum of the order parameter Δ_{max} to T_c reflect the same behavior. If the Fermi energy is sufficiently far away from 0, the ratios plummet at $g = g_{enh}$. As before, $2\Delta_{true}/T_c$ remains at a low value as the energy gap is not affected by the order parameter far away from the Fermi edge. The value $E_F = -0.1W$ presents an interesting marginal case. Here, the ratios never drop. Yet, there is a kink in $2\Delta_{max}/T_c$, when $|\Delta(\varepsilon_{peak})| > |\Delta(E_F)|$. As before, the energy gap itself remains unaffected. Hence, $2\Delta_{true}/T_c$ remains smooth, but decreases substantially due to the increased critical temperature.

Next, we turn to the calculations of the specific heat C_V plotted in Fig. 19. For Fig. 19(a), we set $E_F = -0.3W$ and essentially find the same behavior as in the main text: For $g < g_{enh}$, C_V behaves in the BCS fashion, while for $g > g_{enh}$, C_V initially increases and then drops discontinuously. This discontinuity smears out for sufficiently large g when the enhanced and conventional contributions to the order parameter overlap. This overlap occurs much faster for $E_F = -0.2W$ in Fig. 19(b). Moreover, the overlap is considerably larger, which is why the valley of low values of C_V disappears almost entirely for large g.

As in the main text, we proceed by evaluating the two-particle response functions $\mathcal{G}_\alpha(\omega)$ with respect to the operators in Eq. (7b). The calculation is done using the iterated equations of motion approach [26]. Figure 20 depicts the spectral functions $\mathcal{A}_\alpha(\omega) := (1/\pi)\mathcal{G}_\alpha(\omega)$, with (a) $\alpha =$ Higgs and (b) $\alpha =$ Phase. The columns depict the data for (1) $E_F = -0.3W$, (2) $E_F = -0.2W$, and (3) $E_F = -0.1W$.

The collective mode associated with the enhanced order can be well distinguished for $E_F = -0.3W$ and $E_F = -0.2W$. Within the quasiparticle continuum, the mode smears out more and more the closer the Fermi energy is shifted to ε_{peak}. It disappears completely for $E_F = -0.1W$. This has to be the case since the conventional and the enhanced order cannot be separated for $E_F = \varepsilon_{peak}$.

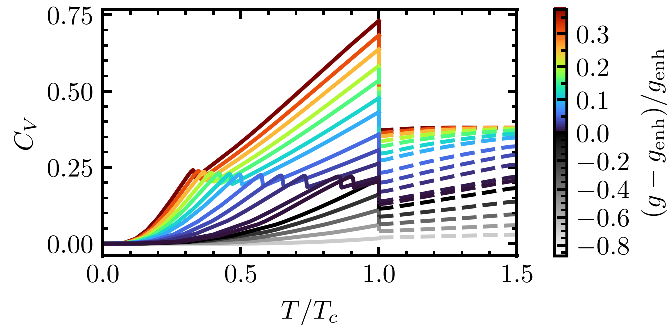

(a) $E_F = -0.3W$, $g_{enh} \approx 1.83$

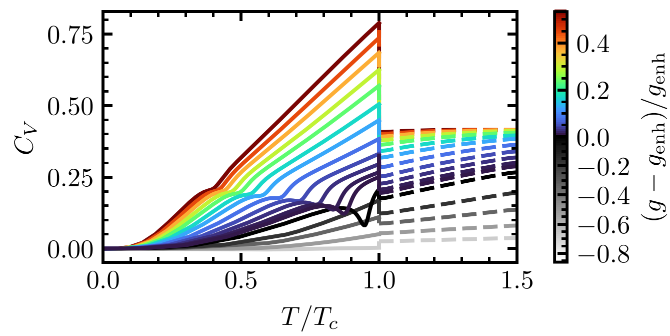

(b) $E_F = -0.2W$, $g_{enh} \approx 1.62$

FIG. 19. Same as Fig. 17 except that E_F is varied.

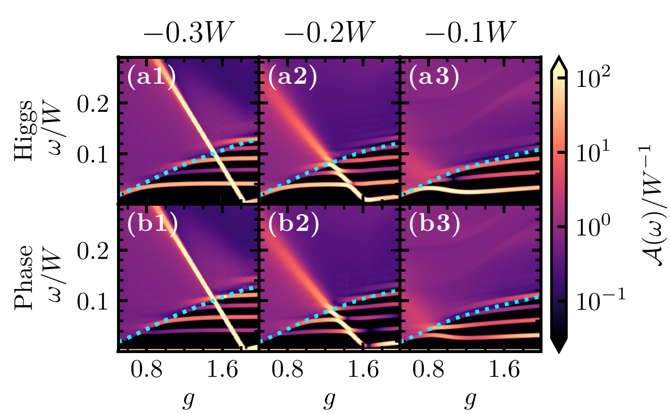

FIG. 20. Calculated zero temperature spectral functions (a) $\mathcal{A}_{Higgs}(\omega)$ and (b) $\mathcal{A}_{Phase}(\omega)$, represented by the color scale. The energy varies along the y axis, and the interaction strength g along the x axis. The cyan dotted line marks the lower edge of the quasiparticle continuum at $2\Delta_{true}$. The artificial broadening is done as in Fig. 4 of the main text. The columns depict the data for (1) $E_F = -0.3W$, (2) $E_F = -0.2W$, and (3) $E_F = -0.1W$. The secondary modes found in Ref. [11] are clearly visible. Additionally, another mode rapidly decreases in energy for $E_F = -0.3W$ and $E_F = -0.2W$. Within the continuum, the mode is less dominant than in the main text and does not soften completely.

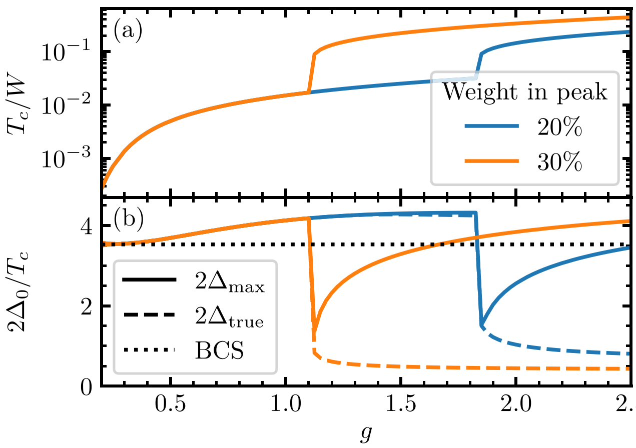

FIG. 21. Same as Fig. 16, except that we consider the rectangular DOS (E1). The blue (orange) lines correspond to the case where the central peak contains 20% (30%) of the DOS's total weight.

Thus, the spectroscopic features, just as the thermodynamic ones, are robust to variations of E_{F} up to a certain degree. Moreover, this analysis corroborates the statements made in the main text that the absence of overlap between enhanced and conventional order causes the sharpness of the collective mode even inside the continuum.

APPENDIX E: A NONDIVERGENT DOS

The phenomenon of enhanced superconductivity does not hinge on the logarithmic singularity of the chosen DOS. It merely requires that the DOS has a large portion of its weight accumulated beyond the Fermi level. To corroborate this claim, we introduce the artificial DOS

$$\rho_{\mathrm{peaked}}(\varepsilon) = \frac{\Theta(W - |\varepsilon|) + \frac{CW}{w}\Theta(w - |\varepsilon|)}{2W(1+C)}. \tag{E1}$$

Here, $\Theta(x)$ is the Heaviside function and $2w$ is the width of the central peak. We fix $w = 0.01W$. The parameter C can be adjusted such that a certain percentage of the DOS's total weight is contained in the range $\varepsilon \in [-w, w]$. Manifestly, this DOS is constant except for a rectangular, nondivergent peak around $\varepsilon = 0$. A plot of this DOS is shown in Fig. 22. The blue (orange) line marks the DOS with 20% (30%) of its weight concentrated in the peak.

In Fig. 21, we show T_c for this choice of DOS. The blue (orange) lines correspond to the case where the central peak contains 20% (30%) of the DOS's total weight. Clearly, the same enhancement as for the bcc DOS occurs here as well. As is to be expected, the enhancement manifests at smaller g if the peak contains more weight. This shows that a logarithmic divergence in the DOS is not necessary to obtain enhanced superconductivity. The accumulation of DOS away from the Fermi level is the crucial aspect.

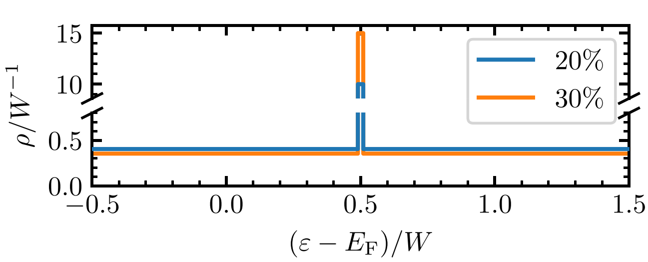

FIG. 22. Nondivergent DOS according to Eq. (E1). The blue (orange) line marks the DOS with 20% (30%) of its weight concentrated in the peak.

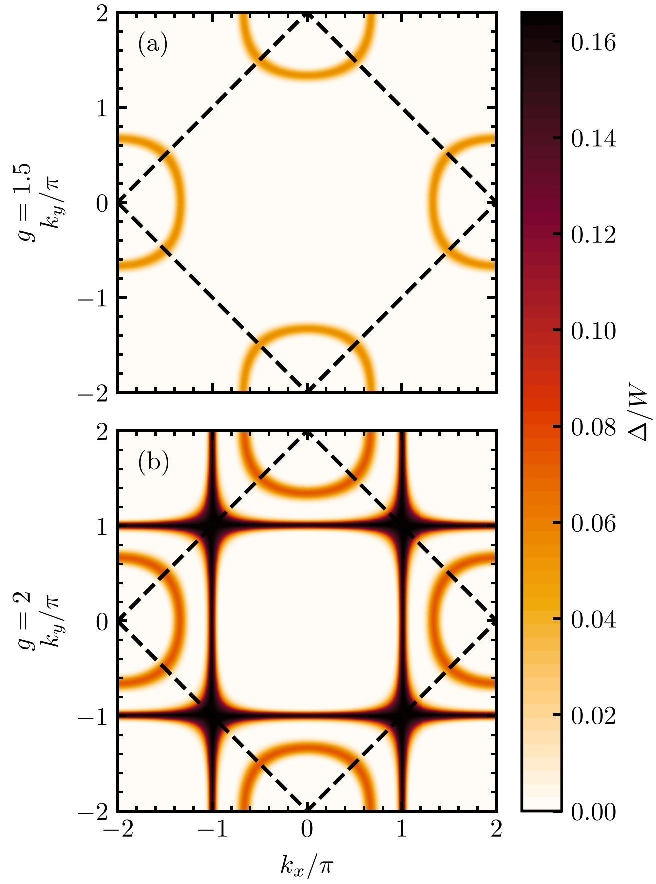

FIG. 23. Order parameter Δ as a function of the momentum. We fix $k_z = 0$. The color scale represents $\Delta(\boldsymbol{k})$. The dotted lines mark the boundary of the first Brillouin zone. We set (a) $g = 1.5 < g_{\mathrm{enh}}$ and (b) $g = 2 > g_{\mathrm{enh}}$.

APPENDIX F: ENHANCED ORDER IN MOMENTUM SPACE

In view of various momentum-resolved experimental techniques, we additionally provide a plot of the order parameter in momentum space in Fig. 23. For clarity, we fixed $k_z = 0$. The color scale represents $\Delta(\boldsymbol{k})$, and the dotted lines mark the boundary of the first Brillouin zone. The top panel (a) depicts the results for $g = 1.5 < g_{\mathrm{enh}}$. Herein, we can easily identify the almost circular shape as the conventional order because the Fermi level is located at these momenta.

The bottom panel (b) shows the results for $g = 2 > g_{\mathrm{enh}}$. Naturally, we find the same conventional order as in panel (a), albeit with a slightly larger magnitude due to the stronger coupling. As for the location of the enhanced contribution, we note that the electron dispersion $\varepsilon(\boldsymbol{k}) \propto \prod_{\alpha\in\{x,y,z\}} \cos(k_\alpha/2)$ originates from $k_\alpha = \pm\pi$. Since the bcc DOS is peaked at $\varepsilon = 0$, the enhanced order appears in the vicinity of $k_\alpha = \pm\pi$.

[1] J. Bardeen, L. N. Cooper, and J. R. Schrieffer, Theory of superconductivity, Phys. Rev. **108**, 1175 (1957).

[2] G. M. Éliashberg, Interactions between electrons and lattice vibrations in a superconductor, J. Exptl. Theoret. Phys. (U.S.S.R.) **38**, 966 (1960) [Sov. Phys. JETP **11**, 696 (1960)].

[3] D. J. Scalapino, J. R. Schrieffer, and J. W. Wilkins, Strong-coupling superconductivity. I, Phys. Rev. **148**, 263 (1966).

[4] C. R. Leavens, Important parameters in strong-coupling superconductivity, J. Phys. F: Met. Phys. **7**, 1911 (1977).

[5] R. Combescot and G. Varelogiannis, The gap over critical temperature ratio $2\Delta/T_c$ in Eliashberg theory, Solid State Commun. **93**, 113 (1995).

[6] C. Joas, I. Eremin, D. Manske, and K. H. Bennemann, Theory for phonon-induced superconductivity in MgB_2, Phys. Rev. B **65**, 132518 (2002).

[7] A. V. Chubukov, A. Abanov, I. Esterlis, and S. A. Kivelson, Eliashberg theory of phonon-mediated superconductivity—When it is valid and how it breaks down, Ann. Phys. **417**, 168190 (2020).

[8] E. A. Yuzbashyan and B. L. Altshuler, Breakdown of the Migdal-Eliashberg theory and a theory of lattice-fermionic superfluidity, Phys. Rev. B **106**, 054518 (2022).

[9] H. Tajima, H. Aoki, A. Perali, and A. Bianconi, Emergent Fano-Feshbach resonance in two-band superconductors with an incipient quasiflat band: Enhanced critical temperature evading particle-hole fluctuations, Phys. Rev. B **109**, L140504 (2024).

[10] J. Lorenzana and G. Seibold, Undamped Higgs modes in strongly interacting superconductors, Condens. Matter **9**, 38 (2024).

[11] J. Althüser and G. S. Uhrig, Collective modes in superconductors including Coulomb repulsion, SciPost Phys. **19**, 067 (2025).

[12] H. Fröhlich, Interaction of electrons with lattice vibrations, Proc. R. Soc. London A **215**, 291 (1952).

[13] P. Lenz and F. Wegner, Flow equations for electron-phonon interactions, Nucl. Phys. B **482**, 693 (1996).

[14] A. Mielke, Calculating critical temperatures of superconductivity from a renormalized Hamiltonian, Europhys. Lett. **40**, 195 (1997).

[15] A. Mielke, Similarity renormalization of the electron-phonon coupling, Ann. Phys. **509**, 215 (1997).

[16] S. Kehrein, Interacting Many-Body Systems, in *The Flow Equation Approach to Many-Particle Systems*, Springer Tracts in Modern Physics, edited by G. Höhler, A. Fujimori, C. Varma, F. Steiner, J. Kühn, J. Trümper, P. Wölfle, and T. Müller (Springer, Berlin, Heidelberg, 2006), Vol. 217.

[17] H. Krull, N. A. Drescher, and G. S. Uhrig, Enhanced perturbative continuous unitary transformations, Phys. Rev. B **86**, 125113 (2012).

[18] J. P. Carbotte, Properties of boson-exchange superconductors, Rev. Mod. Phys. **62**, 1027 (1990).

[19] G. S. Joyce, Exact evaluation of the body centred cubic lattice Green function, J. Phys. C **4**, 1510 (1971).

[20] P. Morel and P. W. Anderson, Calculation of the superconducting state parameters with retarded electron-phonon interaction, Phys. Rev. **125**, 1263 (1962).

[21] E. P. Wohlfarth and P. Rhodes, Collective electron metamagnetism, Philos. Mag. **7**, 1817 (1962).

[22] G. Czycholl, *Theoretische Festkörperphysik: Von den klassischen Modellen zu modernen Forschungsthemen*, Springer-Lehrbuch (Springer, Berlin, Heidelberg, 2008).

[23] M. Sigrist, Introduction to unconventional superconductivity, AIP Conf. Proc. **789**, 165 (2005).

[24] M. Kostrzewa, R. Szczęśniak, J. K. Kalaga, and I. A. Wrona, Anomalously high value of Coulomb pseudopotential for the H_5S_2 superconductor, Sci. Rep. **8**, 11957 (2018).

[25] M. Simonato, M. I. Katsnelson, and M. Rösner, Revised Tolmachev-Morel-Anderson pseudopotential for layered conventional superconductors with nonlocal Coulomb interaction, Phys. Rev. B **108**, 064513 (2023).

[26] J. Althüser and G. S. Uhrig, Collective excitations in competing phases in two and three dimensions, Phys. Rev. B **109**, 205153 (2024).

[27] G. S. Uhrig, Interaction quenches of Fermi gases, Phys. Rev. A **80**, 061602 (2009).

[28] M. Kalthoff, F. Keim, H. Krull, and G. S. Uhrig, Comparison of the iterated equation of motion approach and the density matrix formalism for the quantum Rabi model, Eur. Phys. J. B **90**, 97 (2017).

[29] P. Bleicker and G. S. Uhrig, Strong quenches in the one-dimensional Fermi-Hubbard model, Phys. Rev. A **98**, 033602 (2018).

[30] L. Schwarz, B. Fauseweh, and D. Manske, Momentum-resolved analysis of condensate dynamic and Higgs oscillations in quenched superconductors with time-resolved ARPES, Phys. Rev. B **101**, 224510 (2020).

[31] D. Pekker and C. M. Varma, Amplitude/Higgs modes in condensed matter physics, Annu. Rev. Condens. Matter Phys. **6**, 269 (2015).

[32] A. P. Schnyder, D. Manske, and A. Avella, Resonant generation of coherent phonons in a superconductor by ultrafast optical pump pulses, Phys. Rev. B **84**, 214513 (2011).

[33] H. Krull, D. Manske, G. S. Uhrig, and A. P. Schnyder, Signatures of nonadiabatic BCS state dynamics in pump-probe conductivity, Phys. Rev. B **90**, 014515 (2014).

[34] L. Schwarz, B. Fauseweh, N. Tsuji, N. Cheng, N. Bittner, H. Krull, M. Berciu, G. S. Uhrig, A. P. Schnyder, S. Kaiser, and D. Manske, Classification and characterization of nonequilibrium Higgs modes in unconventional superconductors, Nat. Commun. **11**, 287 (2020).

[35] R. A. Barankov and L. S. Levitov, Excitation of the dissipationless Higgs mode in a fermionic condensate, arXiv:0704.1292.

[36] J. Lorenzana and G. Seibold, Long-lived Higgs modes in strongly correlated condensates, Phys. Rev. Lett. **132**, 026501 (2024).

[37] G. Rickayzen, *Green's Functions and Condensed Matter*, Techniques of Physics, Vol. 5 (Academic Press, London, 1980).

[38] A. V. Chubukov, I. Eremin, and D. V. Efremov, Superconductivity versus bound-state formation in a two-band superconductor with small Fermi energy: Applications to Fe pnictides/chalcogenides and doped $SrTiO_3$, Phys. Rev. B **93**, 174516 (2016).

[39] C. Wen, Z. Hou, A. Akbari, K. Chen, W. Hong, H. Yang, I. Eremin, Y. Li, and H.-H. Wen, Unprecedentedly large gap in

$HgBa_2Ca_2Cu_3O_{8+\delta}$ with the highest T_c at ambient pressure, npj Quantum Mater. **10**, 20 (2025).

[40] Y. in 't Veld, M. I. Katsnelson, A. J. Millis, and M. Rösner, Enhancing plasmonic superconductivity in layered materials via dynamical Coulomb engineering, npj 2D Mater. Appl. **10**, 30 (2026).

[41] E. A. Pashitskii and V. I. Pentegov, On the plasmon mechanism of high-T_c superconductivity in layered crystals and two-dimensional systems, Low Temp. Phys. **34**, 113 (2008).

[42] V. Z. Kresin and H. Morawitz, Layer plasmons and high-T_c superconductivity, Phys. Rev. B **37**, 7854 (1988).

[43] J. Althüser, I. M. Eremin, and G. S. Uhrig, Enhanced superconductivity in proximity to peaks in densities of states, TUDOdata, 2026, https://doi.org/10.17877/TUDODATA-2026-ML9IYD6F.

[44] A. Mielke, Flow equations for band-matrices, Eur. Phys. J. B **5**, 605 (1998).

[45] C. Knetter and G. Uhrig, Perturbation theory by flow equations: Dimerized and frustrated S = 1/2 chain, Eur. Phys. J. B **13**, 209 (2000).

[46] C. Heidbrink and G. Uhrig, Renormalization by continuous unitary transformations: One-dimensional spinless fermions, Eur. Phys. J. B **30**, 443 (2002).